


ARTICLE

Remote ischemic post-conditioning promotes hematoma resolution via AMPK-dependent immune regulation

Kumar Vaibhav¹, Molly Braun¹, Mohammad Badruzzaman Khan², Sumbul Fatima³, Nancy Saad⁴, Adarsh Shankar⁵, Zenab T. Khan¹, Ruth B.S. Harris⁶, Qiu Hua Yang⁷, Yuqing Huo⁷, Ali S. Arbab⁵, Shailendra Giri⁸, Cargill H. Alleyne Jr.¹, John R. Vender¹, David C. Hess², Babak Baban^{2,4,9}, Md Nasrul Hoda^{2,3}, and Krishnan M. Dhandapani¹ 

Spontaneous intracerebral hemorrhage (ICH) produces the highest acute mortality and worst outcomes of all stroke subtypes. Hematoma volume is an independent determinant of ICH patient outcomes, making clot resolution a primary goal of clinical management. Herein, remote-limb ischemic post-conditioning (RIC), the repetitive inflation–deflation of a blood pressure cuff on a limb, accelerated hematoma resolution and improved neurological outcomes after ICH in mice. Parabiosis studies revealed RIC accelerated clot resolution via a humoral-mediated mechanism. Whereas RIC increased anti-inflammatory macrophage activation, myeloid cell depletion eliminated the beneficial effects of RIC after ICH. Myeloid-specific inactivation of the metabolic regulator, AMPKα1, attenuated RIC-induced anti-inflammatory macrophage polarization and delayed hematoma resolution, providing a molecular link between RIC and immune activation. Finally, chimera studies implicated myeloid CD36 expression in RIC-mediated neurological recovery after ICH. Thus, RIC, a clinically well-tolerated therapy, noninvasively modulates innate immune responses to improve ICH outcomes. Moreover, immunometabolic changes may provide pharmacodynamic blood biomarkers to clinically monitor the therapeutic efficacy of RIC.

Introduction

Spontaneous intracerebral hemorrhage (ICH) results from the rupture of small vessels damaged by chronic hypertension or amyloid angiopathy. The subsequent extravasation of erythrocytes produces a dynamic, space-occupying intracranial hematoma that is associated with mechanical tissue destruction, edema development, elevated intracranial pressure, enhanced microvascular compression, regional cerebral hypoperfusion, and poor clinical outcomes (Qureshi et al., 2001; Gebel et al., 2002; Christoforidis et al., 2007). Hematoma volume also is strongly correlated with the severity of white matter injury in ICH patients (Lou et al., 2010). The Guidelines for the Management of Spontaneous ICH in Adults recommend surgical clot evacuation in neurologically deteriorating patients (Class IIb, Level of Evidence C) and in patients presenting with lobar clots >30 ml and within 1 cm from the surface (Class IIb, Level of Evidence B; Hemphill et al., 2015); however,

the benefits of neurosurgical clot evacuation remain unclear for most ICH patients (Class IIb, Level of Evidence A; Hemphill et al., 2015). Along these lines, the multi-center, randomized Surgical Trial in ICH failed to observe an overall benefit of early surgical hematoma evacuation in supratentorial ICH, as compared with conservative management (Mendelow et al., 2005). Similarly, the effectiveness of stereotactic or endoscopic clot aspiration with thrombolytic usage remains uncertain (Class IIb, Level of Evidence B; Nguyen et al., 1992; Teernstra et al., 2003; Thiex et al., 2004; Barrett et al., 2005; Marquardt et al., 2005; Gregson et al., 2012). As such, medical management remains the standard of care for most ICH patients, leading to the designation of ICH as the least treatable form of stroke.

In the absence of surgical evacuation, intact erythrocytes persist within the parenchyma for days after ICH (2–3 d in ro-

¹Department of Neurosurgery, Medical College of Georgia, Augusta University, Augusta, GA; ²Department of Neurology, Medical College of Georgia, Augusta University, Augusta, GA; ³Department of Medical Laboratory, Imaging, and Radiological Sciences, College of Allied Health Sciences, Augusta University, Augusta, GA; ⁴Department of Oral Biology, Dental College of Georgia, Augusta University, Augusta, GA; ⁵Department of Biochemistry and Molecular Biology, Medical College of Georgia, Augusta University, Augusta, GA; ⁶Department of Physiology, Medical College of Georgia, Augusta University, Augusta, GA; ⁷Department of Cellular Biology and Anatomy, Medical College of Georgia, Augusta University, Augusta, GA; ⁸Department of Neurology, Henry Ford Health System, Detroit, MI; ⁹Department of Surgery, Medical College of Georgia, Augusta University, Augusta, GA.

Correspondence to Krishnan M. Dhandapani: KDHANDAPANI@augusta.edu.

© 2018 Vaibhav et al. This article is distributed under the terms of an Attribution–Noncommercial–Share Alike–No Mirror Sites license for the first six months after the publication date (see <http://www.rupress.org/terms/>). After six months it is available under a Creative Commons License (Attribution–Noncommercial–Share Alike 4.0 International license, as described at <https://creativecommons.org/licenses/by-nc-sa/4.0/>).

dents; 5–10 d in humans) before hemolytic breakdown (Darrow et al., 1988; Xi et al., 1998; Huang et al., 2002). Hemolysis aids in intrinsic clot resolution, yet the simultaneous liberation of heme products elevates brain-free iron concentrations, increases oxidative damage, and exacerbates neurological injury (Sadrzadeh et al., 1987; Letarte et al., 1993; Chiu et al., 1996; Huffman et al., 2000; Yip and Sastry, 2000; Bhasin et al., 2002; Nakamura et al., 2005, 2006; Lyden et al., 2007; Han et al., 2008; Shen et al., 2008; Qing et al., 2009). Thus, erythrocyte removal during the acute and sub-acute phase of injury may profoundly improve both acute and long-term patient prognoses. Macrophages are professional phagocytes that engulf pathogens and cellular debris after infection or tissue injury. Central nervous system (CNS) infiltration of peripheral macrophages temporally and spatially correlated with spontaneous hematoma clearance after ICH (Zhao et al., 2007; Hammond et al., 2012), suggesting a potential role for innate immune mediators in neurological recovery after ICH. Macrophages polarize along a continuum, based on microenvironmental cues, to generate divergent, context-specific functions. In support of this assertion, “classically activated” macrophages release pro-inflammatory cytokines to remove damaged cells from sites of injury, yet chronic activation exacerbates secondary damage and impairs tissue repair (Mantovani et al., 2005). Conversely, “alternatively activated” macrophages release anti-inflammatory cytokines to dampen immune responses and to promote wound healing (Gordon and Martinez, 2010). Interestingly, alternatively activated macrophages were correlated with acute hematoma resolution in mice (Chang et al., 2017). Moreover, elevated total leukocyte counts were associated with a higher risk of developing white matter lesions (Kim et al., 2011), and elevations in classically activated macrophages predicted relapsing white matter injury after experimental multiple sclerosis (Mikita et al., 2011). These findings suggest the identification of clinically amenable therapeutic approaches that enhance alternatively activated macrophage activity may accelerate hematoma resolution and improve long-term ICH patient outcomes.

Transient bouts of “sub-lethal” ischemia, delivered either before or after an insult, increased tissue resiliency in multiple models of ischemia-reperfusion injury via a process deemed ischemic conditioning (Murry et al., 1986; Yellon and Hausenloy, 2005; Crisostomo et al., 2006). More recently, remote-limb ischemic post-conditioning (RIC), the repetitive inflation-deflation of a blood pressure cuff on a limb, noninvasively reduced ischemic tissue damage (Andreka et al., 2007). RIC was efficacious in clinical trials for myocardial infarction (Bøtker et al., 2010) and intracranial stenosis (Meng et al., 2012) and was well tolerated in both acute ischemic stroke (England et al., 2017) and subarachnoid hemorrhage patients (Koch et al., 2011; Gonzalez et al., 2013, 2014), with no adverse effects on coagulation profiles (Mayor et al., 2013). While these early stage clinical trials are indicative of the safety, versatility, and translational potential of RIC in critically ill patients, the utility for nonischemic brain injuries, including ICH, is undemonstrated. Interestingly, remote ischemic preconditioning shifted the metabolic profile after experimental myocardial infarction and in patients undergoing elective aortic valve replacement (Chao de la Barca et al., 2016). Consistent with

these observations, activation of the metabolic sensor, 5' adenosine monophosphate-activated protein kinase (AMPK), correlated with cardioprotection after ischemic preconditioning in rabbits (Nishino et al., 2004), although the functional implications were unexplored. As changes in cellular metabolism regulate immune effector responses (Pearce and Pearce, 2013), we hypothesized that RIC improves neurological outcomes via immunometabolic regulation after ICH.

Results

RIC accelerates spontaneous hematoma resolution after ICH

To test the hypothesis that RIC improves ICH outcomes, a collagenase injury model was used to recapitulate the spontaneous vascular rupture and dynamic hematoma expansion observed after clinical ICH. Initiation of once-daily bilateral RIC beginning at 2 h after ICH, which transiently reduced hind limb blood flow to ~65–70% of baseline during cuff inflation with a return to 100% of baseline upon cuff deflation (Fig. S1), reduced hematoma volume by 43% ($P < 0.001$ vs. mock conditioning; Fig. 1A) and improved cerebral blood flow by 24% ($P < 0.001$ vs. mock conditioning), as compared with mock-conditioned mice after ICH (Fig. 1B) at day 5 after injury. Conversely, no statistically significant differences in either hematoma volume or cerebral perfusion were observed at 24 or 72 h after ICH (Fig. S2), suggesting RIC accelerated hematoma resorption rather than attenuated clot formation/expansion. In line with this assertion, RIC reduced hematoma volume by 47% at 6 d following intracerebral placement of a fixed volume of autologous blood ($P < 0.05$ vs. mock conditioning; Fig. 1, C and D). In contrast, RIC did not affect total hematoma volume at day 3 in the autologous blood model, although migration of blood toward the cerebral ventricles was prominent at this earlier time point (Fig. 1, C and D), potentially reflecting an early step in hematoma clearance.

The presence of an intrastriatal hematoma is associated with functional deficits in motor coordination; thus, we next assessed the effect of RIC on neurological improvement. Delivery of once-daily RIC beginning at 2 h after ICH reduced focal deficits ($P < 0.001$ vs. ICH with mock conditioning) and normalized the left/right swing ratio in an elevated body swing test ($P < 0.01$ vs. ICH with mock conditioning, not significantly different from sham) at day 5 after ICH (Fig. 2A), demonstrating a role for RIC in improving asymmetry motor behavior after collagenase-induced ICH. RIC also induced a 34% reduction in the time required to transverse a narrow beam ($P < 0.05$ vs. ICH with mock conditioning, not significantly different from sham; Fig. 2A), further demonstrating a functional improvement in motor coordination by RIC. These findings were mirrored by enhanced outcomes in the open field test, which assesses general locomotion and anxiety. Specifically, RIC normalized distance traveled and movement velocity to levels observed in sham-operated mice ($P < 0.05$ vs. ICH with mock conditioning, not significantly different from sham; Fig. 2B). In addition, RIC increased the frequency of time spent in the center zones ($P < 0.05$ vs. ICH with mock conditioning, not significantly different from sham), suggesting a reduction in anxious behavior after ICH with RIC treatment (Fig. 2B). The ability of RIC to improve behavioral outcomes after colla-

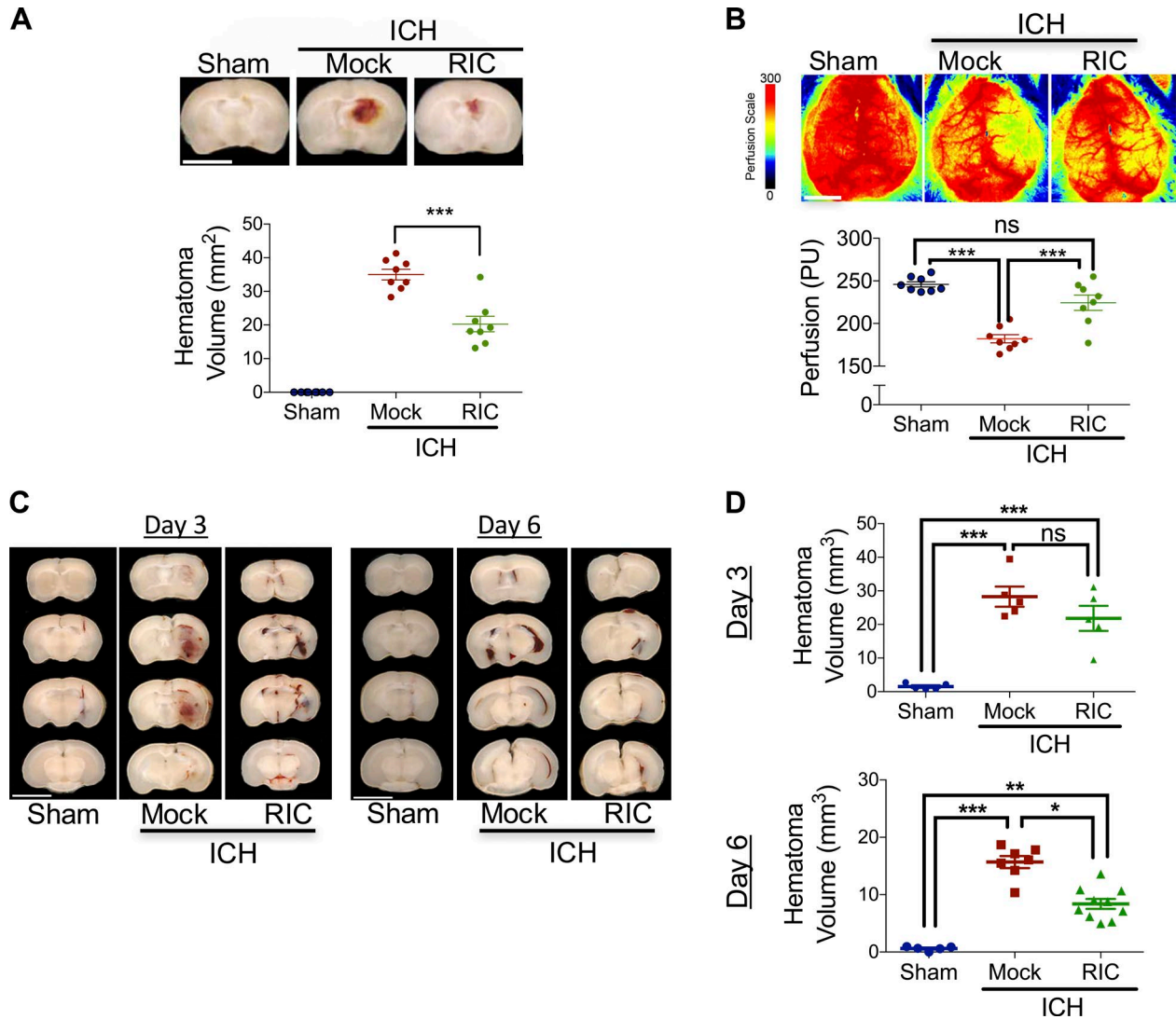


Figure 1. RIC promotes delayed hematoma resolution and improves outcomes after ICH. (A) Mixed sex C57BL/6J littermates were randomized to receive once-daily mock conditioning or bilateral RIC beginning at 2 h after sham or collagenase-induced ICH. At day 5, hematoma area was quantified in serial 2-mm coronal slices. Bar, 4 mm. Data are mean \pm SEM from $n = 8$ mice/group and were analyzed by one-way ANOVA followed by Tukey's post-hoc test (***, $P < 0.001$). Data are representative of two independent experiments. (B) Mixed sex C57BL/6J littermates were randomized to receive once-daily mock conditioning or bilateral RIC beginning at 2 h after sham or collagenase-induced ICH. At day 5, peri-hematoma blood flow was assessed by laser speckle contrast imaging. Bar, 4 mm. Data are mean \pm SEM from $n = 8$ mice/group and were analyzed by one-way ANOVA followed by Tukey's post-hoc test (***, $P < 0.001$; ns, not statistically significant). Data are representative of two independent experiments. (C and D) Mixed sex C57BL/6J littermates were randomized to receive once-daily mock conditioning or bilateral RIC beginning at 2 h after sham or intrastriatal placement of 30 μ l autologous blood. Littermates were randomized to receive once-daily mock conditioning or bilateral RIC beginning at 2 h after ICH. At day 3 and 6 after injury, hematoma area was quantified in serial 2-mm coronal slices. Bar, 4 mm. Data are mean \pm SEM from $n = 5$ –10 mice/group and were analyzed by one-way ANOVA followed by Tukey's post-hoc test (*, $P < 0.05$; **, $P < 0.01$; ***, $P < 0.001$; ns, not statistically significant). Data are representative of two independent experiments.

genase-induced ICH paralleled similar effects in the autologous blood model of ICH. Along these lines, RIC reduced the time required to transverse the narrow beam by 77% ($P < 0.001$ vs. mock conditioning, not significantly different from sham) and produced a 46% improvement on the grip strength test ($P < 0.05$ vs. mock conditioning), as compared with mock-conditioned mice after ICH (Fig. 2 C).

RIC improves ICH outcomes via innate immune modulation

We explored the mechanisms whereby noninvasive cuff inflation on a remote limb accelerated hematoma resolution within the CNS. To ascertain whether humoral factors mediated the

observed effects, we generated parabiotic pairs that allow blood exchange between surgically conjoined mice (Fig. 3, A and B). RIC on the uninjured pair-mate accelerated hematoma clearance in the injured pair-mate whereas mock conditioning was ineffective (Fig. 3, B and C). As these data implicated circulating factors, rather than direct neural stimulation, in neurovascular improvement by RIC, we next sought to identify the factor(s) underlying these beneficial effects after ICH.

Professional phagocytes remove damaged cells and debris after injury and macrophage infiltration temporally correlated with hematoma resolution after experimental ICH. To establish a causative role in accelerating hematoma resolution by RIC, we

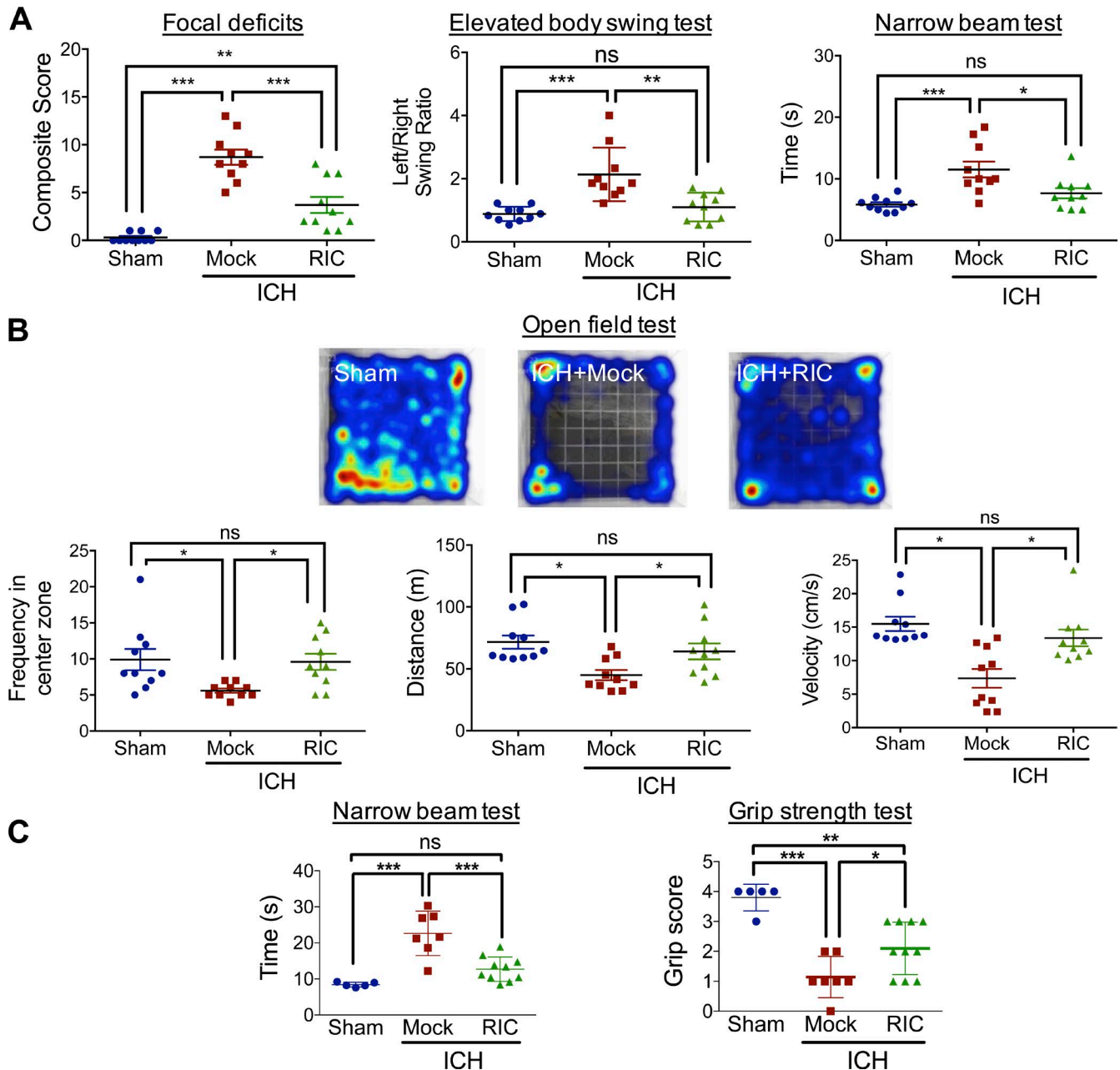


Figure 2. RIC improves neurobehavioral outcomes after ICH. Mixed sex C57BL/6J littermates were randomized to receive once-daily mock conditioning or bilateral RIC beginning at 2 h after sham or collagenase-induced ICH. **(A)** Neurological outcomes were assessed at day 4–5 after injury, using a composite focal deficits score (a measure of global injury severity), the elevated body swing test (a task of asymmetric motor behavior), and by the narrow beam test (a measure of motor balance and coordination). Data are mean \pm SEM from $n = 10$ mice/group and were analyzed by one-way ANOVA followed by Tukey’s post-hoc test (*, $P < 0.05$; **, $P < 0.01$; ***, $P < 0.001$; ns, not statistically significant). Data are representative of two independent experiments. **(B)** Mixed sex C57BL/6J littermates were randomized to receive once-daily mock conditioning or bilateral RIC beginning at 2 h after sham or collagenase-induced ICH. At day 4 after injury, neurological outcomes were assessed using the open field test. Representative heat maps are depicted, and frequency in the center zone, distance traveled, and movement velocity were quantified. Data are mean \pm SEM from $n = 10$ mice/group and were analyzed by one-way ANOVA followed by Tukey’s post-hoc test (*, $P < 0.05$; ns, not statistically significant). Data are representative of two independent experiments. **(C)** Mixed sex C57BL/6J littermates were randomized to receive once-daily mock conditioning or bilateral RIC beginning at 2 h after sham or intrastriatal placement of 30 μ l autologous blood. Neurobehavioral outcomes, including the narrow beam test and grip strength test, were assessed at day 6 after injury. Data are mean \pm SEM from $n = 5$ –10 mice/group and were analyzed by one-way ANOVA followed by Tukey’s post-hoc test (*, $P < 0.05$; **, $P < 0.01$; ***, $P < 0.001$; ns, not statistically significant). Data are representative of two independent experiments.

selectively depleted >92% of myeloid cells using clodronate-encapsulated liposomes (clodrosome) before sham/ICH (Fig. 4 A). Whereas administration of empty liposomes (encapsome) did not affect RIC-mediated clot resolution or edema formation

(Fig. 4 B), clodrosome administration delayed intrinsic clot resolution and completely reversed the beneficial effect of RIC on both hematoma clearance and edema development (Fig. 4 B). Consistent with a functional role for infiltrating macrophages

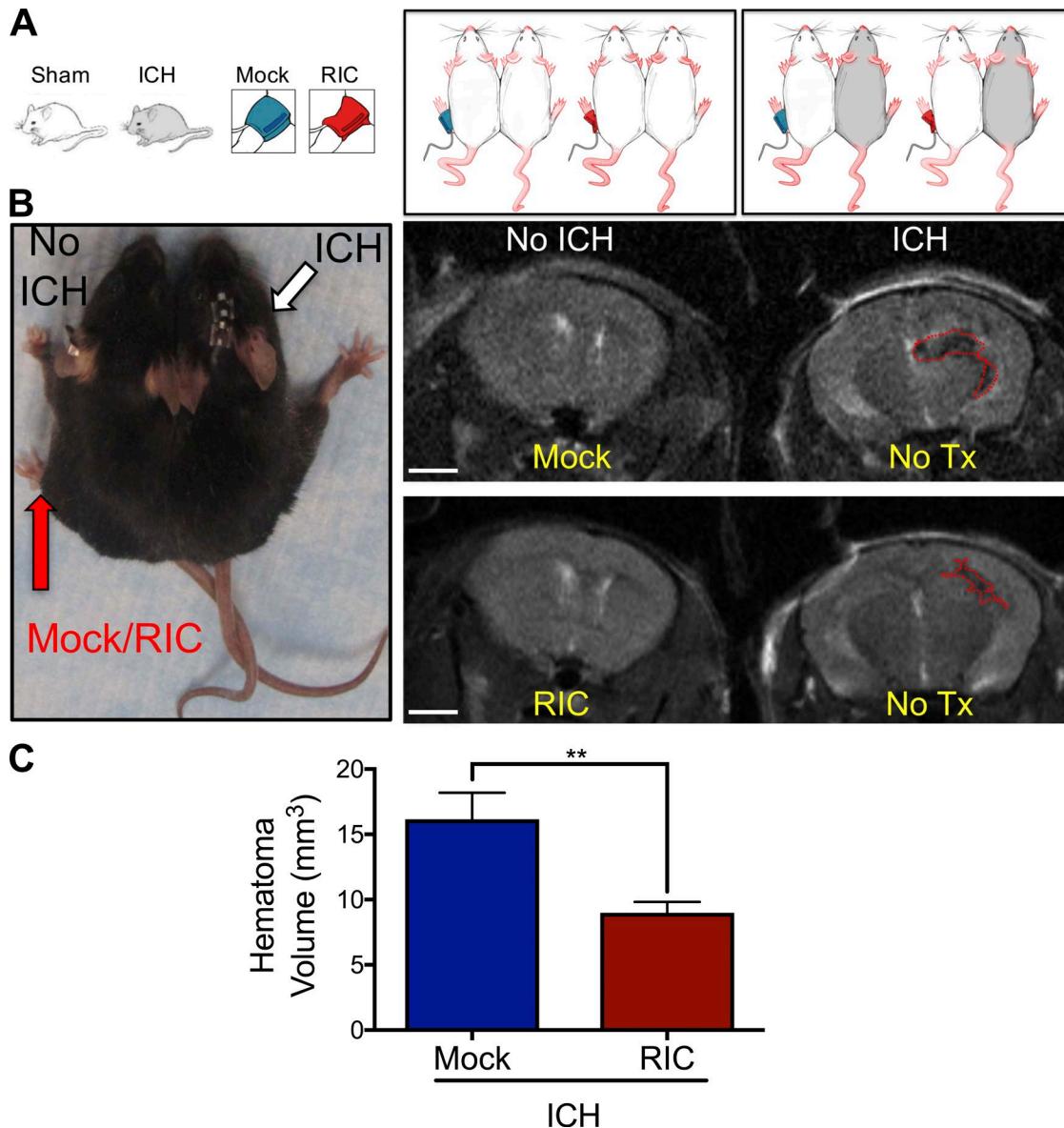


Figure 3. Humoral factors mediate RIC-induced hematoma resolution. (A) Parabolic pairs ($n = 6$ pairs/group) were generated using age-matched male C57BL/6j mice and randomized to treatment arms, as illustrated. In all pairs, the left pair mate was treated with either once-daily mock conditioning or RIC for 5 d without injury. The right pair mate was untreated and received either a sham injury or ICH. (B) Photograph of a representative parabolic pair (left). Mock conditioning or RIC was performed in the left pair mate and sham/ICH was performed on the right pair mate, as indicated. Representative MRI brain scans at day 5 after ICH (right). The brain on the left side is uninjured, and the perimeter of the hematoma is indicated by a red dotted line in the brain on the right side. Bar, 2 mm. (C) Quantification of hematoma volume, as assessed by MRI. Data are mean \pm SEM from $n = 6$ pairs/treatment group. Data are representative of two independent experiments and were analyzed by Student's t test (**, $P < 0.01$).

in neurological recovery, RIC-mediated hematoma resolution was absent in $CCR2^{-/-}$ mice, but not in WT mice, at day 5 after ICH (Fig. S3, A and B). Further analysis of peri-hematoma brain tissue revealed a reduction in the accumulation of $CD11b^{+}$, $CD45^{+}$ -infiltrated macrophages in $CCR2^{-/-}$ mice after ICH. Myeloid expression of the scavenger receptor, $CD36$, was blunted in $CCR2^{-/-}$ mice, as compared with WT mice; however, we did not observe any differences between WT and $CCR2^{-/-}$ mice in the regulation of $F4/80$, $Ly-6C^{low}$, or $Ly-6C^{hi}$ myeloid cells following RIC (Fig. S3, C and D).

To further investigate the contribution of macrophages toward RIC-induced recovery, CFSE-labeled donor macrophages were

intravenously administered to recipient mice immediately after injury. Whereas the absolute number of infiltrating macrophages was unaffected, RIC induced an injury-independent polarization of CFSE-labeled macrophages toward an anti-inflammatory ($CFSE^{+}$, $CD11b^{+}$, $F4/80^{+}$, $CD206^{+}$, $IL-10^{+}$) phenotype, as compared with mock-conditioned mice (Fig. 5, A–C). Conversely, pro-inflammatory ($CFSE^{+}$, $CD11b^{+}$, $CD206^{-}$, $F4/80^{+}$, $TNF-\alpha^{+}$) macrophages were either unchanged or decreased in blood or brain, respectively, by RIC (Fig. 5, A–C). In line with these data obtained using CFSE-labeled macrophages, RIC increased the expression $CD11b^{+}$, $CD206^{+}$, $IL-10^{+}$ anti-inflammatory macrophages, but not $CD11b^{+}$, $CD206^{-}$, $TNF-\alpha^{+}$ pro-inflammatory macrophages, in parabiotics (Fig. 5 D).

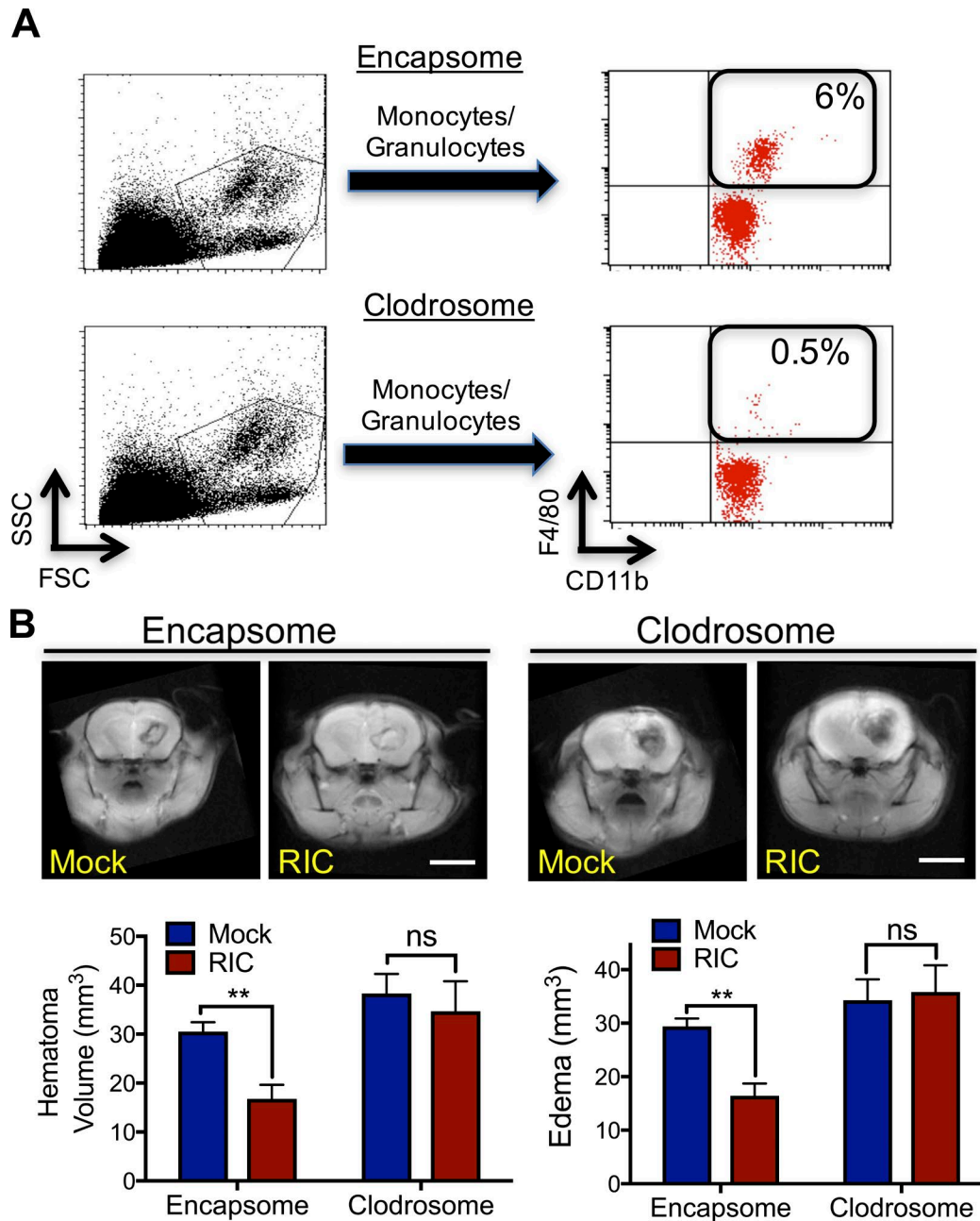


Figure 4. Macrophage activation is required for RIC-induced hematoma resolution after ICH. (A) Control liposomes (encapsome) or clodronate liposomes (clodrosome) were administered intraperitoneally to mixed sex C57BL/6J littermates for three consecutive days to deplete myeloid cells. Monocyte/granulocyte populations were identified using FSC/side scatter (SSC) and myeloid cell depletion was quantified in CD11b⁺, F4/80⁺ myeloid cells. Inset numbers indicate the percentage of total blood cells. Data are representative of $n = 8$ mice/group from two independent experiments. (B) Mixed sex C57BL/6J littermates were administered either encapsome or clodrosome for three consecutive days, as indicated in A. Mice were then randomized to receive once-daily mock conditioning or bilateral RIC beginning at 2 h after collagenase-induced ICH. Hematoma volume and edema volume were quantified by MRI at day 5 after ICH. Bar, 4 mm. Data are mean \pm SEM from $n = 8$ /group and were analyzed using a Student's t test (**, $P < 0.01$; ns, not statistically significant). Data are representative of two independent experiments.

The shift toward an anti-inflammatory macrophage phenotype suggests potential utility for RIC as a prophylactic treatment and/or as a post-injury intervention to establish a favorable niche for tissue recovery. Moreover, RIC significantly increased the expression of both CD206 ($P < 0.0001$) and IL-10 ($P < 0.0001$) in infiltrated CD11b⁺, CD45^{HI} brain macrophages, as compared with mock conditioning after ICH (Fig. 6). We also observed increased

myeloid expression of the scavenger receptor, CD36, in both circulating CD11b⁺, CD68⁺ monocytes ($P < 0.05$ vs. mock conditioning) and CD11b⁺, CD45^{HI} brain-infiltrated macrophages ($P < 0.001$ vs. mock conditioning) after ICH (Fig. 6) and a selective elevation in the expression of MerTK, which is implicated in myelin phagocytosis, in brain-infiltrated macrophages after ICH ($P < 0.01$ vs. mock conditioning). In contrast, RIC did not significantly affect

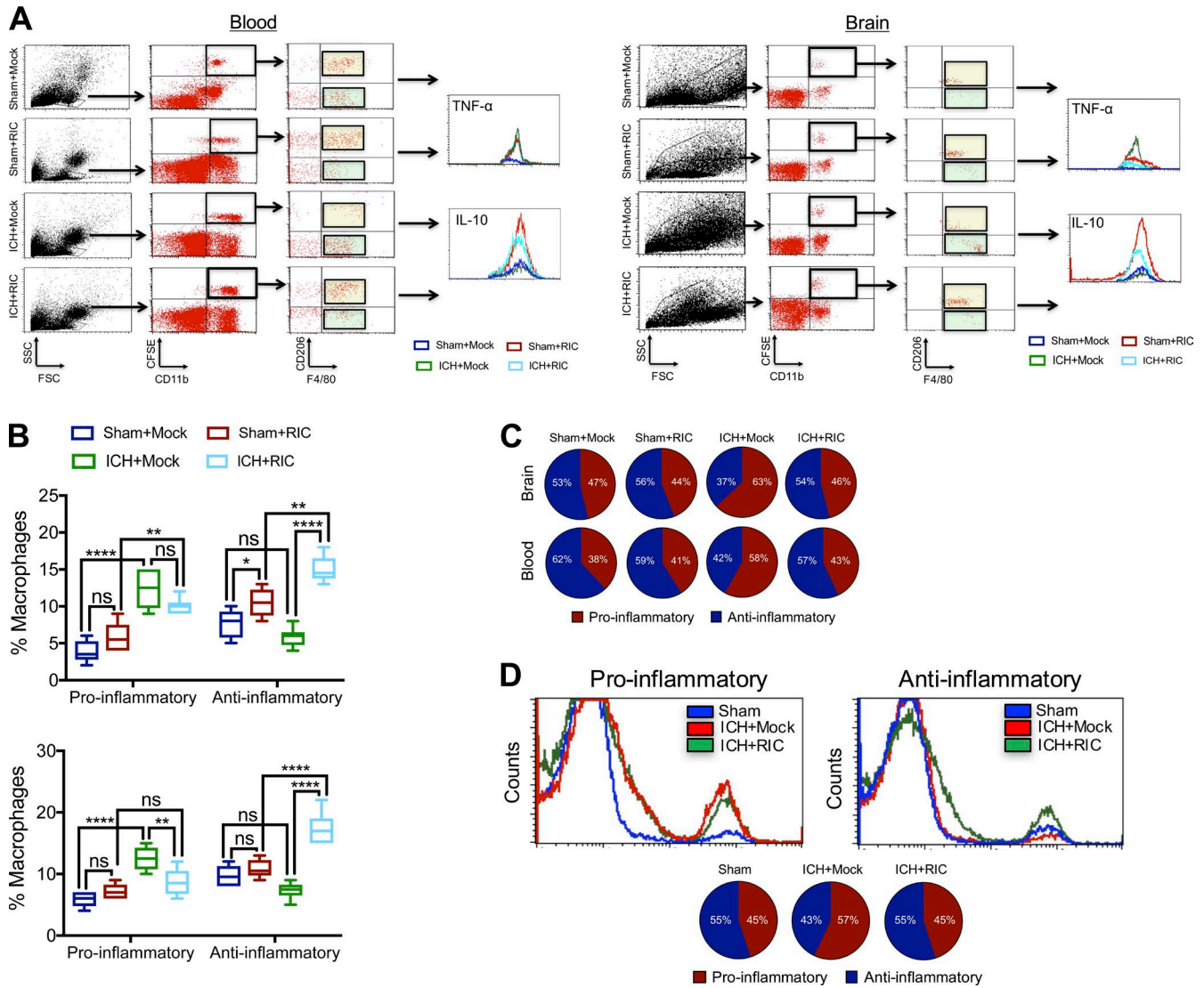


Figure 5. RIC promotes anti-inflammatory macrophage polarization. (A and B) CFSE-labeled donor macrophages were intravenously administered (5×10^5 cells/recipient) to male C57BL/6J littermates at 1 h after sham or collagenase-induced ICH. Mice were randomized to receive once-daily mock or RIC beginning at 2 h after injury, and both blood and brain tissue were collected at 72 h after sham/ICH. Live cells were gated according to the FSC/SSC profile and further gating was performed to detect $CD11b^+$, $CFSE^+$ cells populations. The effect of RIC on the phenotype of blood and brain macrophages were further defined as anti-inflammatory ($CFSE^+$, $CD11b^+$, $F4/80^+$, $CD206^+$, $IL-10^+$) or pro-inflammatory ($CFSE^+$, $CD11b^+$, $CD206^+$, $F4/80^+$, $TNF-\alpha^+$). Data are mean \pm SEM from $n = 6$ mice/group and were analyzed by one-way ANOVA followed by Tukey's post-hoc test (**, $P < 0.01$; ****, $P < 0.0001$; ns, not statistically significant). Data are representative of two independent experiments. (C) Graphic representation of the ratio of pro-inflammatory/anti-inflammatory macrophages, as determined in B. (D) Representative histograms and graphic representation of the ratio of pro-inflammatory/anti-inflammatory macrophages in blood collected from parabiotic pairs, as defined in A. Data are mean \pm SEM from $n = 6$ pairs/group and are representative of two independent experiments.

the myeloid expression of MHC-II, Ly6G, or Ly6C in either blood or brain macrophages after traumatic brain injury (Fig. 6).

Myeloid AMPK α 1 is necessary for RIC-induced hematoma resolution

Myeloid cells expressed the AMPK catalytic subunit, AMPK α 1, but not the AMPK α 2 subunit (Fig. 7 A). AMPK α 1 was basally phosphorylated in the brain of sham-operated mice, whereas an 88% reduction in phosphorylated AMPK α 1 was observed in mock-conditioned mice after ICH ($P < 0.001$ vs. sham; Fig. 7 B). RIC increased phosphorylated AMPK α 1 by 1.9-fold and 1.7-fold within $CD11b^+$, $F4/80^+$ -infiltrated myeloid cells after ICH, as com-

pared with both sham-operated mice ($P < 0.01$) and mock-conditioned ICH mice ($P < 0.01$), respectively (Fig. 7, B and C). Next, we analyzed the effect of RIC on the phenotype of $CD11b^+$, $CD45^{hi}$ -infiltrated brain macrophages in myeloid-specific AMPK α 1 knockout mice (Fig. S4). Whereas RIC did not significantly affect myeloid expression of either $F4/80$, Ly6G, or MHC-II following sham or ICH in either WT or myeloid-specific AMPK α 1 knockout mice, an ICH-dependent increase in the expression of both $CD36$ ($P < 0.01$ vs. mock conditioned ICH mice) and MerTK ($P < 0.01$ vs. mock conditioned ICH mice) was observed following RIC (Fig. 7 D). These RIC mediated changes were not observed in sham-injured mice (not significantly different from mock con-

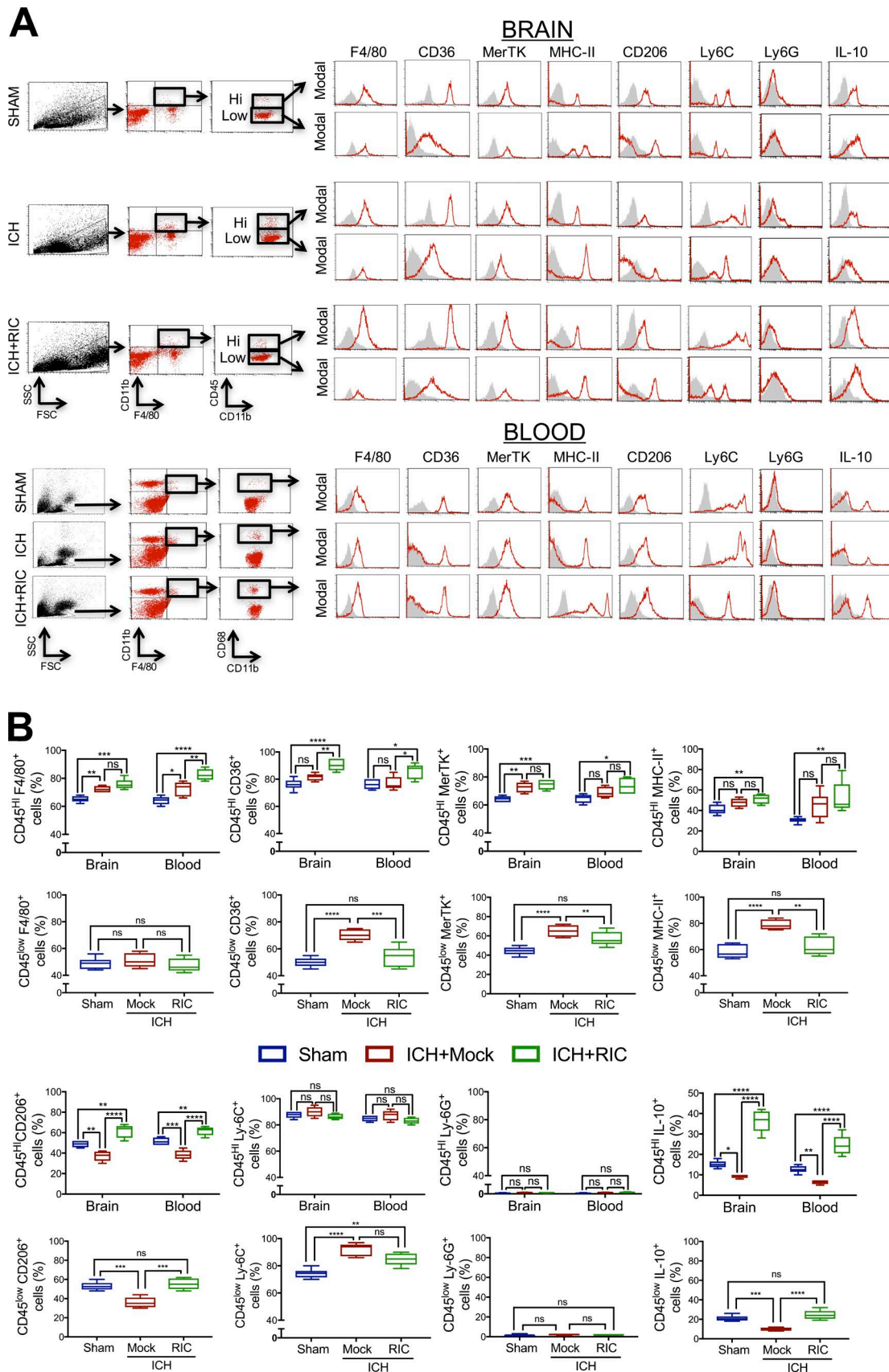


Figure 6. **RIC induces anti-inflammatory macrophage polarization after ICH.** (A and B) Mixed sex C57BL/6J littermates were randomized to receive once-daily mock conditioning or bilateral RIC beginning at 2 h after sham or collagenase-induced ICH. Phenotypic analysis of macrophages was performed in peri-hematoma brain tissue (0.2 g) or blood (B; 200 μ l) at 72 h after sham, ICH with mock conditioning (ICH), or ICH+RIC. Live cells were gated using FSC/SSC

ditioning), nor did RIC induce these effects in myeloid-specific AMPK α 1 knockout mice (not significantly different from mock conditioning; Fig. 7 D). Notably, RIC did not significantly affect the expression of CD206, a widely used marker of anti-inflammatory macrophages, or IL-10, a key regulatory cytokine, in either sham-operated WT or myeloid-specific AMPK α 1 knockout mice. In contrast, RIC produced an AMPK α 1-dependent increase in myeloid IL-10 expression following ICH ($P < 0.0001$ vs. mock conditioning in WT ICH mice; not significantly different from mock conditioning in myeloid-specific AMPK α 1 knockout mice), while RIC similarly increased CD206 expression in both genotypes after ICH ($P < 0.0001$ vs. mock conditioned ICH mice of both genotypes; Fig. 7 D). In parallel to these changes, the beneficial effects of RIC on hematoma resolution and edema development were eliminated in myeloid-specific AMPK α 1 knockout mice, as compared with WT mice (Fig. 7 E). Moreover, the improvements in motor function (e.g., narrow beam test, grim strength test, elevated body swing test) observed following RIC were eliminated in myeloid-specific AMPK α 1 knockout mice (Fig. S5), implicating myeloid AMPK α 1 as a key molecular switch responsible for neurological recovery after RIC.

Myeloid CD36 mediates hematoma resolution and white matter sparing after RIC

To demonstrate a causative role for myeloid CD36 in intrinsic clot resolution, irradiation bone marrow chimera studies were used whereby myeloid CD36 was completely eliminated (Fig. 8 A). Whereas transplantation of CD36 knockout (CD36 $^{-/-}$) bone marrow into WT recipient mice (CD36 $^{-/-}$ \gg WT) eliminated the protective ability of RIC on hematoma resolution and edema development, introduction of WT bone marrow into irradiated CD36 $^{-/-}$ (WT \gg CD36 $^{-/-}$) mice led to a 53% reduction in hematoma volume ($P < 0.05$ vs. mock conditioning) and 53% reduction in edema formation ($P < 0.05$ vs. mock conditioning; Fig. 8 B). Lastly, we explored the long-term effects of RIC on white matter damage. RIC attenuated long-term white matter loss after ICH, with prominent protection observed in white matter regions adjacent to the resolved hematoma, including the lateral corpus callosum, fimbria, and internal capsule (Fig. 9, A–D). The ability of RIC to prevent white matter loss was observed throughout the corpus callosum and fimbria of WT \gg CD36 $^{-/-}$ chimera mice (Fig. 9 E). RIC also spared white matter in CD36 $^{-/-}$ \gg WT chimera mice, albeit to a lesser magnitude and over a smaller anatomical region as compared with WT \gg CD36 $^{-/-}$ mice (Fig. 9 E). In line with these findings, RIC failed to prevent ventricular enlargement, an anatomical measure of cognitive impairment, in CD36 $^{-/-}$ \gg WT chimera mice whereas ventricular size was reduced in WT \gg CD36 $^{-/-}$ mice (Fig. 9 F). Thus, myeloid CD36 expression may be critical for the ability of RIC to enhance both acute and long-term neurological function after ICH.

Discussion

ICH, a severe neurological injury that produces 1-yr mortality rates of 60%, is associated with the recovery of functional independence in $<20\%$ of survivors after 6 mo (Dennis et al., 1993; Gebel et al., 2002; Dennis, 2003; Weimar et al., 2003; Rincon and Mayer, 2004; Broderick et al., 2007). This poor prognosis has remained unchanged for decades, and no FDA-approved therapies presently exist to enhance quality of life among ICH survivors. As the incidence of ICH is expected to double over the next several decades due to an aging population and changes in racial demographics (Rincon and Mayer, 2004), there is a dire need for efficacious interventions to improve patient outcomes. In this study, we used diverse in vivo approaches to identify RIC as a safe, noninvasive, and clinically feasible therapy to modulate innate immune activation and accelerate hematoma resolution in two clinically relevant mouse models of ICH.

An important, yet unexpected, observation was that innate immune modulation mechanistically linked the repetitive cuff inflation–deflation on a remote limb with hematoma resolution after ICH. Specifically, the beneficial effects of RIC were dependent on AMPK, an energy-sensing, serine/threonine kinase that functions as a cellular metabolic switch. Emerging evidence suggests immunometabolic changes, including increased glucose uptake, elevated glycolysis, and enhanced activation of the pentose phosphate pathway, mechanistically define inflammatory activation and polarization (O'Neill and Hardie, 2013). That RIC selectively activated myeloid AMPK α 1 to enhance anti-inflammatory macrophage polarization is in line with reports showing AMPK inhibits fatty acid synthesis, a key regulatory pathway of pro-inflammatory macrophage polarization (Biswas and Mantovani, 2012), in bovine mammary epithelial cells (McFadden and Corl, 2009). Our findings also are supported by data showing global AMPK α 1 deletion impaired anti-inflammatory signaling in response to IL-10 and amplified pro-inflammatory myeloid activity, whereas AMPK activation increased pro-inflammatory macrophage polarization (Sag et al., 2008; Carroll et al., 2013; Zhu et al., 2015; Mangalam et al., 2016). In addition to demonstrating a mechanistic role for AMPK in restraining pro-inflammatory activation, our data implicate RIC as a clinically amenable therapy to restore activated AMPK and to polarize innate immune responses toward a reparative, anti-inflammatory phenotype. Our findings also suggest that the assessment of myeloid metabolic status may provide a simple, pharmacodynamic biomarker to monitor the biological response to RIC. Similarly, an increased ratio of anti-inflammatory/pro-inflammatory macrophages may provide an alternative and easily obtained surrogate blood biomarker of therapeutic efficacy after RIC.

Myeloid cell depletion prevented both spontaneous and RIC-induced hematoma resolution after ICH, supporting a role for macrophages in tissue repair and phagocytosis. CD36 is an

and CD11b $^{+}$ F4/80 $^{+}$ cells were further selected. CD11b $^{+}$ CD45 hi -infiltrated myeloid cells and CD11b $^{+}$ CD45 low residential myeloid cells were selected from brain tissue, or CD11b $^{+}$ CD68 $^{+}$ macrophages were selected from blood. Selected populations were further defined using F4/80, CD36, MerTK, MHC-II, CD206, Ly-6C, Ly-6G, or IL-10. Representative histograms are provided for each marker. Gray shaded areas indicate isotype controls. Quantified data, which are expressed as the mean \pm SEM from $n = 6$ mice/group, were analyzed using a one-way ANOVA followed by Tukey's post-hoc test (*, $P < 0.05$; **, $P < 0.01$; ***, $P < 0.001$; ****, $P < 0.0001$; ns, not statistically significant) and are representative of two independent experiments.

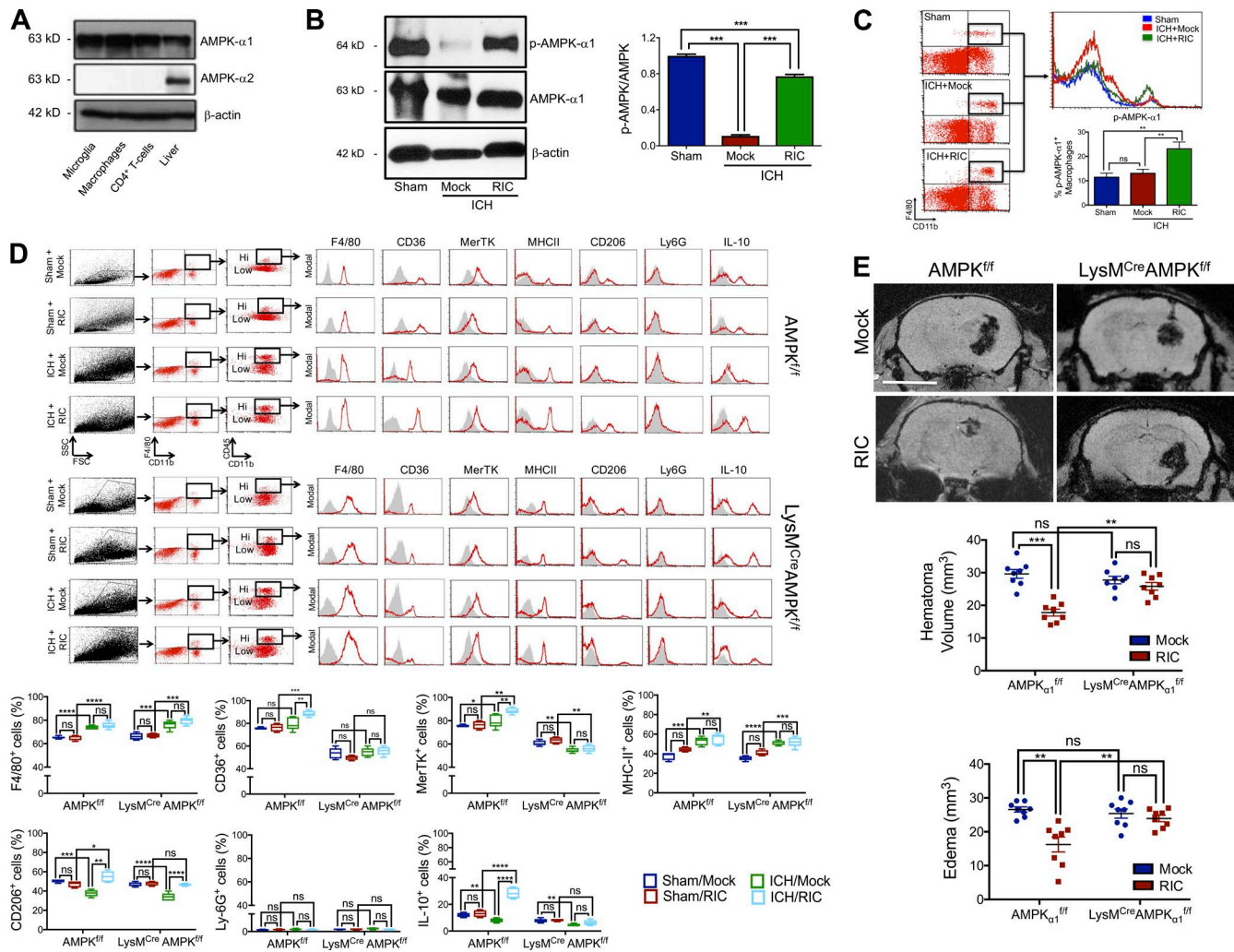


Figure 7. Myeloid AMPK α 1 mediates hematoma resolution after RIC. (A) Western blot analysis of AMPK α 1 and AMPK α 2 subunits in microglia, macrophages, CD4⁺ T cells, and liver (positive control). β -actin was used as a loading control. (B) Phosphorylated AMPK α 1/2 (p-AMPK α 1/2) and total AMPK α were assessed in brain tissue of male C57BL/6J mice at day 5 after sham/ICH by Western blotting. Densitometry analysis, which are expressed as the mean \pm SEM from *n* = 6 mice/group, were analyzed using a one-way ANOVA followed by Tukey's post-hoc test (***, *P* < 0.001; ns, not statistically significant) and are representative of two independent experiments. (C) Phosphorylated AMPK α 1 (p-AMPK α 1) was assessed in brain tissue of male C57BL/6J mice at day 5 after sham/ICH by flow cytometry. Data are expressed as the mean \pm SEM from *n* = 6 mice/group and were analyzed using a one-way ANOVA followed by Tukey's post-hoc test (**, *P* < 0.01; ns, not statistically significant). Data are representative of two independent experiments. (D) Mixed sex WT (AMPK α 1^{f/f}) or myeloid-specific AMPK α 1 knockout (LysM^{Cre}AMPK α 1^{f/f}) littermates were randomized to sham/collagenase-induced ICH groups and received either mock conditioning or RIC beginning at 2 h after injury. At 72 h after injury, macrophages were phenotypically defined in peri-hematoma brain tissue (0.2 g) after sham, sham + RIC, ICH with mock conditioning, or ICH+RIC. Live cells were gated using FSC/SSC and CD11b⁺F4/80⁺ cells were selected. CD11b⁺CD45^{hi}-infiltrated macrophages were further defined using F4/80, CD36, MerTK, MHC-II, CD206, Ly-6G, or IL-10. Representative histograms are provided for each marker and isotype controls are indicated by gray shaded areas. Data from two independent experiments are expressed as the mean \pm SEM from *n* = 6 mice/group and were analyzed using a one-way ANOVA followed by Tukey's post-hoc test (*, *P* < 0.05; **, *P* < 0.01; ***, *P* < 0.001; ****, *P* < 0.0001; ns, not statistically significant). (E) Mixed sex AMPK α 1^{f/f} or LysM^{Cre}AMPK α 1^{f/f} littermates were randomized to sham/collagenase-induced ICH groups and received either mock conditioning or RIC beginning at 2 h after injury. At day 5 after sham/ICH, hematoma volume and edema were assessed by MRI. Representative images are shown and quantified data are mean \pm SEM from *n* = 8 mice/group. Bar, 4 mm. Data were analyzed using a one-way ANOVA followed by Tukey's post-hoc test (**, *P* < 0.01; ***, *P* < 0.001; ns, not statistically significant) and are representative of three independent experiments.

integral cell membrane protein and type B scavenger receptor expressed by multiple cells types that mediates phagocytosis of erythrocytes, as well as damaged and senescent cells (Zhao et al., 2007, 2015; Flores et al., 2016). Interestingly, patients with a CD36 deletion exhibit delayed hematoma resorption and worse neurological outcomes after ICH, while global genetic deletion of CD36 attenuated clot absorption after experimental ICH in mice (Fang et al., 2014). While implicating CD36 as a critical mediator

of hematoma resorption after a brain hemorrhage, translational approaches to exploit the therapeutic potential of CD36 are lacking. Consistent with reports showing AMPK activation increases the membrane translocation of CD36 (Samovski et al., 2012), the ability of RIC to increase CD36 expression in brain-infiltrated macrophages was lost in myeloid-specific AMPK α 1 knockout mice after ICH. Coupled with our chimera studies that demonstrated a critical, functional role for myeloid CD36 expression in

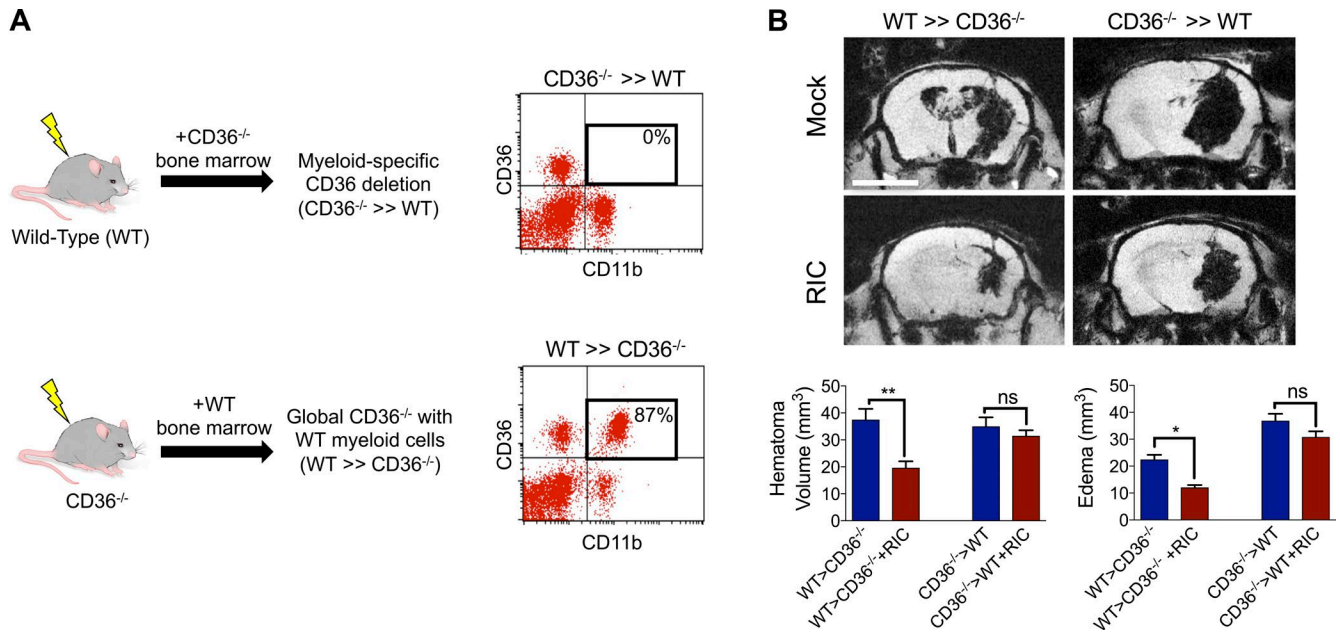


Figure 8. Myeloid CD36 mediates hematoma resolution by RIC. (A) Schematic depicting the generation of myeloid-specific CD36 knockout mice using an irradiation bone marrow chimera approach. Male WT (C57BL/6j) or CD36^{-/-} mice were irradiated and reconstituted using bone marrow from either genotype, as indicated. Flow cytometric analysis of blood (200 μ l) collected from mice at 4 wk after bone marrow transplant, showing successful generation of chimeric mice following transplantation of CD36^{-/-} bone marrow into irradiated WT mice (CD36^{-/-} >> WT) or transplantation of WT bone marrow into irradiated CD36^{-/-} mice (WT >> CD36^{-/-}). Inset numbers represent the percentage of CD36⁺, CD11b⁺ myeloid cells. **(B)** WT >> CD36^{-/-} mice and CD36^{-/-} >> WT mice were randomized to sham/ICH groups and received either mock conditioning or RIC. At day 5 after sham/ICH, MRI was used to assess hematoma volume and cerebral edema. Bar, 4 mm. Representative images are depicted and data are expressed as mean \pm SEM from $n = 8$ mice/group. Data were analyzed using a one-way ANOVA followed by Tukey's post-hoc test (*, $P < 0.05$; **, $P < 0.01$; ns = not statistically significant) and are representative of two independent experiments.

RIC-mediated hematoma resolution, RIC may provide a clinically safe approach to harness the protective effects of CD36. Moreover, myeloid expression of CD36 may provide another potential biomarker to monitor acute recovery in peripheral blood after traumatic brain injury.

Beyond the devastating, acute effects of the hematoma, cognitive dysfunction and gait disorders are frequent long-term consequences of white matter injury in ICH survivors (Lee et al., 2010). We reported that global AMPK α 1 knockout mice exhibited severe demyelination in an experimental autoimmune encephalomyelitis model of multiple sclerosis (Mangalam et al., 2016), whereas chronic daily RIC limited white matter loss after experimental vascular cognitive impairment (Khan et al., 2018) and ICH (this study). Notably, administration of anti-inflammatory monocytes reversed active demyelination and supported oligodendrocyte differentiation during CNS remyelination (Miron et al., 2013). As oligodendrocyte precursor cells proliferated and differentiated within white matter tracts after ICH (Joseph et al., 2016), our observed, AMPK-dependent increase in anti-inflammatory macrophage polarization may support both acute (hematoma resolution) and long-term (attenuated white matter loss, remyelination) recovery by RIC after ICH. These important possibilities will be the subject of future mechanistic exploration by our laboratory to better define the optimal timing, duration, and conditions to maximize recovery in ICH patients. These studies also may provide critical information to support the utility of RIC in other acute neurological injuries, such as ischemic stroke and traumatic brain injuries.

Our findings suggest that RIC could be a safe, simple, and effective treatment for intracranial hemorrhages; however, our study possesses several limitations. First, the experimental model used may not accurately mimic all aspects of the human ICH condition. The intrastriatal injection of collagenase recapitulates the spontaneous vascular rupture and hematoma expansion observed in clinical ICH; however, this model induces an exaggerated inflammatory response that may contribute toward neurological injury. To circumvent this issue, we included a second model whereby a fixed volume of autologous blood was directly placed into the striatum. Our proof of concept and early stage translational studies used young, healthy, and genetically similar mice. The inclusion of mice with common comorbidities, such as hypertension and diabetes, are needed to further advance the translational potential of RIC after ICH. Mechanistically defining how transient ischemia alters immunometabolism remains a translational obstacle. Shear stress induced by inflation of the blood pressure cuff likely mediates the observed effects, yet it remains unknown whether these effects occur directly at the level of the immune cell and/or may involve an intermediary cell type. In support of the latter possibility, plasma nitrite, a circulating mediator of RIC (de Lima Portella et al., 2015; Hess et al., 2016), is associated with increased AMPK activation (Kröller-Schön et al., 2012; Lai et al., 2016). Thus, further exploration of the role of the vasculature in mediating the immunoregulatory functions of RIC may be necessary to refine the frequency, duration, and/or optimal cycle number of RIC. Regardless of the mechanism, our findings are consistent with a report showing a single bout

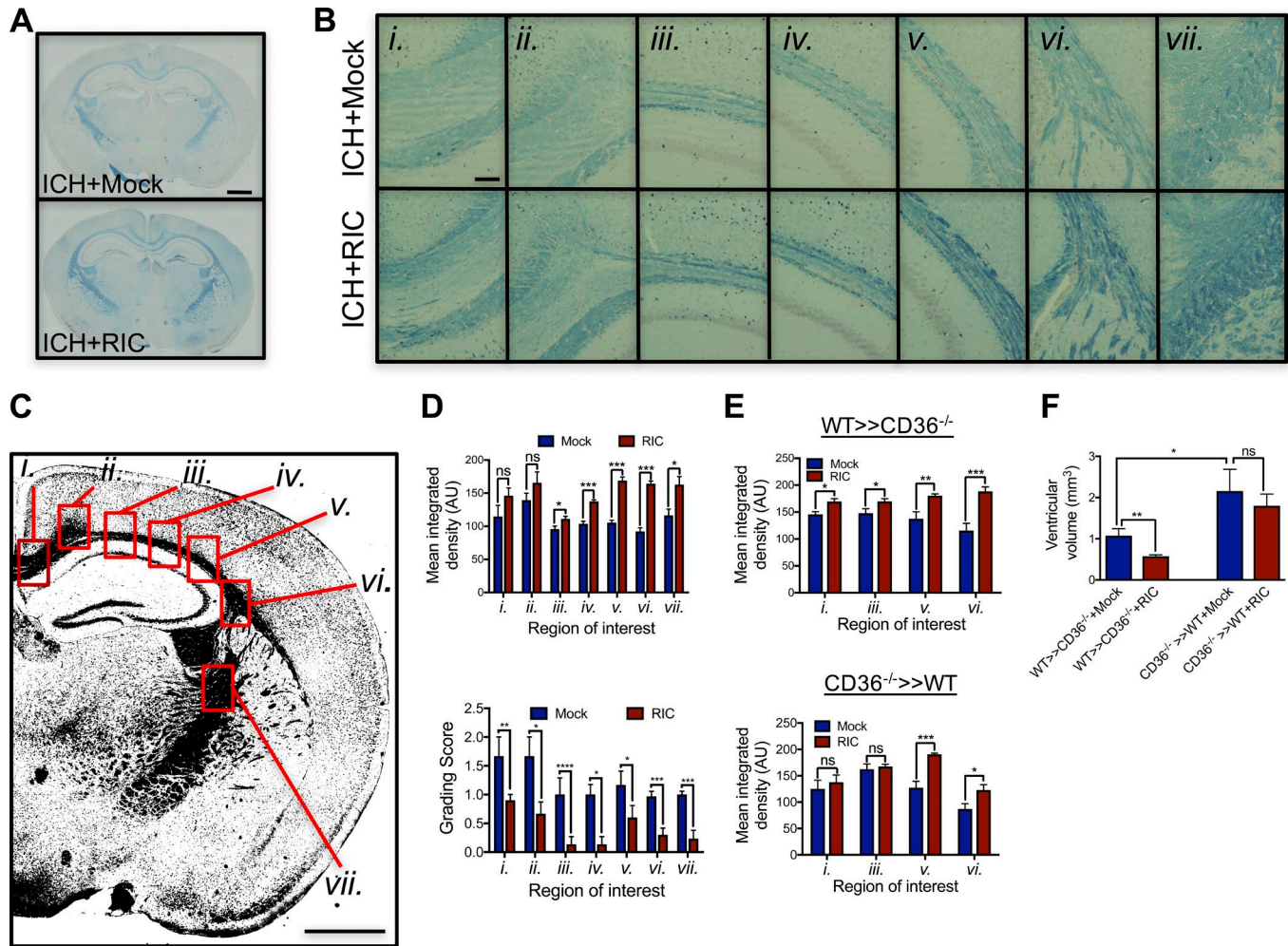


Figure 9. Myeloid-specific deletion of CD36 increases long-term white matter injury after ICH. (A) Mixed sex C57BL/6J littermates were randomized to receive once-daily mock conditioning or bilateral RIC beginning at 2 h after sham or collagenase-induced ICH. White matter was assessed in coronal brain sections by LFB staining at 8 wk after injury. Bar, 1 mm. (B) Sequential micrographs (20× magnification) demonstrate a sparing effect of RIC on white matter after ICH. Bar, 100 μm. Roman numerals (i–vii) denote anatomical locations, as indicated in C. Bar, 1 mm. Data are representative of *n* = 5–7 mice/group from two independent experiments. (D) White matter loss was quantified by mean integrated density and LFB grading score in regions adjacent to the clot location, including the lateral corpus callosum, fimbria, and internal capsule. Representative tissue sections are shown in B (*, *P* < 0.05; **, *P* < 0.01; ***, *P* < 0.001). (E) Male WT >> CD36^{-/-} and CD36^{-/-} >> WT chimera mice were generated, as in Figure 8, randomized to sham/ICH groups, and received either mock conditioning or RIC. At 8 wk after injury, white matter loss was quantified by mean integrated density in selected brain regions. Data are representative of *n* = 6 mice/group from two independent experiments and were analyzed using a one-way ANOVA followed by Tukey's post-hoc test (*, *P* < 0.05; ***, *P* < 0.001; ns, not statistically significant). (F) Ventricular enlargement, a common manifestation of white matter loss, was quantified by fluid attenuation inversion recovery at 1 mo after ICH in WT >> CD36^{-/-} and CD36^{-/-} >> WT chimera mice. Data are mean ± SEM from *n* = 5–7/mice group and were analyzed using a one-way ANOVA followed by Tukey's post-hoc test. Data are representative of two independent experiments.

of RIC (three cycles × 10-min duration) failed to affect hematoma volume in rats when initiated at 1 h after ICH (Geng et al., 2012). More importantly, the regimen of RIC used in this report to modulate macrophage polarization and to accelerate hematoma resolution is identical to the clinical protocol implemented in the phase II remote ischemic conditioning after stroke trial, which showed RIC was safe, well-tolerated, and efficacious in acute ischemic stroke patients (Hess et al., 2015; England et al., 2017).

Based on our findings, RIC may possess broad utility in a variety of other indications beyond ICH, including traumatic brain injury, subdural hematoma, epidural hematoma, and arteriovenous malformations. RIC also may accelerate the recovery of peripheral injuries, including intra-abdominal, peritoneal, splenic,

hepatic, or intramuscular hematomas. Of significance, delivery of a regimen of RIC identical to that used in this report improved the 90-d National Institutes of Health (NIH) Stroke Scale score and reduced vascular events in a pilot randomized placebo controlled trial of 26 acute ischemic stroke patients (13 sham conditioned, 13 RIC; England et al., 2017); however, it is important to note that initiation of RIC was delayed by an average of 15.8 h after ictus and that patients receiving hyperacute stroke treatments, such as stroke thrombolysis, were excluded. With respect to the timing of RIC delivery, a randomized, proof-of-concept clinical trial of paramedic-administered remote ischemic per-conditioning in 443 patients (247 received treatment, 196 received standard of care) exhibiting symptoms of acute stroke revealed an

overall neutral effect, although a significant reduction in tissue risk of infarction was observed (Hougaard et al., 2014). Importantly, in this latter trial designed to assess safety and feasibility, ~18% of patients receiving remote per-conditioning did not complete the full four cycles of inflation and deflation due to a short transport time. Given the apparent importance of cycle number and duration on immunometabolic regulation of macrophages in this study, future clinical investigation may be warranted to further optimize and refine the conditions to maximize the long-term benefits of RIC. Finally, recanalization with thrombolytics is efficacious within a narrow therapeutic window after acute ischemic stroke, but is contraindicated in patients with extra- or intra-axial hemorrhage. As ~15% of patients initially presenting with stroke symptomology are ultimately diagnosed with ICH, time- and resource-intensive radiological confirmation of stroke subtype is required before treatment initiation. Given the simplicity to administer, minimal required training, and lack of required specialized equipment, implementation of RIC immediately upon suspected stroke diagnosis may be warranted, including use during emergency transport, in community/rural hospitals, or within emergency departments to provide an early and critical “low risk, high reward” therapeutic option.

Materials and methods

Study design

The primary objective of this study was to test the hypothesis that RIC is efficacious in experimental models of ICH. A secondary objective was to test the hypothesis that the beneficial effects of RIC were dependent on immunometabolic regulation of macrophage polarization after ICH. Primary study endpoints included hematoma volume, edema, and neurobehavioral outcomes. For all studies, mice were used as the research subject in these controlled laboratory experiments. Studies used a double-blinded study design, and mice were randomized to treatment groups in a predetermined manner by a study coordinator separate from the surgeon. Toward this end, each mouse was ear-tagged with a subject number that was maintained by a blinded study coordinator that was unaware of treatment groups or endpoint. Blinded investigators performed all data acquisition of outcome measures (e.g., magnetic resonance imaging [MRI], behavior, flow cytometry). Following final data acquisition, mice were decoded, and final analyses were performed. Power analysis for one-way ANOVA and *t* test was conducted a priori to determine a sufficient sample size using $\alpha = 0.05$ and $\beta = 0.10$. No experimental subjects were removed from the study, and all data are included in the final analysis.

ICH model

Animal studies were reviewed and approved by the Institutional Animal Care and Use Committee at Augusta University, in compliance with NIH guidelines. A mouse collagenase model of ICH was used for most studies, per our laboratory (Sukumari-Ramesh et al., 2012). In brief, mixed sex C57BL/6J mice (8–10 wk old; Jackson Laboratories, stock no. 004999) or CCR2^{-/-} mice (Jackson Laboratories, stock no. 004999) were placed into a stereotactic frame and a 0.5-mm diameter burr hole was drilled over the pa-

rietal cortex, 2.2 mm lateral to the bregma. A 26-G Hamilton syringe, loaded with 0.04 U of bacterial type IV collagenase in 0.5 μ l saline, was lowered 3 mm deep from the skull surface directly into the left striatum. The syringe was depressed at a rate of 450 nl/min and left in place for several minutes after the procedure to prevent solution reflux and excess diffusion. For the autologous blood injection model, 30 μ l of blood was injected directly into the striatum using a 22-G Hamilton syringe, as we detailed previously. In both models, sham injured mice received intrastriatal administration of saline to control for any tissue damage due to the injection. After the syringe was removed, bone wax was used to close the burr hole, the incision was surgically stapled, and mice were kept warm until recovery of the righting reflex. For all studies, littermates were used to reduce a source of experimental variability.

RIC

An automated blood pressure instrument was modified to produce cuff-based, noninvasive, bilateral RIC in the mouse hind limbs (Hatteras Instruments). Starting at 2 h after ICH (a time point conservatively associated with initial medical evaluation of ICH patients) and continuing daily thereafter, RIC was performed in isoflurane-anesthetized mice, per our group with minor modifications (Hoda et al., 2012). In brief, mice were placed on a thermoregulated bed to maintain body temperature at 37°C and slightly stretched limbs were secured using paper tape. Customized mouse limb cuffs were wrapped on each hind limb, and RIC was performed as four cycles \times 5 min/cycle at 200 mmHg using a 5-min reperfusion interval. Mock-conditioned mice were anesthetized in an identical manner to the RIC group. Mock-conditioned groups were secured in a mouse holder, but the blood pressure cuff was not inflated, controlling for any effects of anesthesia, stress, or handling. This clinically used protocol is well tolerated and does not induce discomfort or distress, as we reported (Hoda et al., 2012). Following the treatment regimen, mice were placed into a clean home cage and monitored until conscious.

Quantification of hematoma volume

Mice were euthanized under deep (5%) isoflurane anesthesia, and 2-mm-thick coronal brain slices were prepared using a mouse brain matrix. Brain slices were imaged using a high-resolution (24 pixels/mm) scanner. Hematoma size was calculated by a blinded investigator using ImageJ version 1.37 software (NIH), as adapted from Vaibhav et al. (2013). In brief, a binary image was created with the hematoma appearing black and remaining brain tissue appearing white (Foerch et al., 2008). Total hematoma area was converted to volume by multiplying by slice thickness and expressed as mean hematoma volume (mm³).

Laser speckle contrast imaging (LSCI)

LSCI was performed as reported by our laboratory (Hoda et al., 2012), with minor modifications. In brief, mice were anesthetized using isoflurane and a midline incision was produced. Perfusion images were acquired using PeriCam high resolution LSCI (PSI system, Perimed) with a 70-mW built-in laser diode for illumination and 1388 \times 1038-pixel charge-coupled device camera installed 10 cm above the skull (speed, 19 Hz; exposure time, 6 ms).

Acquired images were analyzed for dynamic changes in cerebral blood flow using PIMSsoft. As both anesthesia and injury affect cerebral perfusion within the contralateral hemisphere, the absolute value from the ipsilateral side was normalized with the value from contralateral side and calculated as percent change. Body temperature was maintained at $37 \pm 0.5^\circ\text{C}$ throughout the experiment.

MRI

Mice were anesthetized with isoflurane (3% for induction, 1.5% for maintenance in a 2:1 mixture of N_2/O_2) and imaged using a horizontal 7 Tesla BioSpec MRI spectrometer (Bruker Instruments) equipped with a 12-cm self-shielded gradient set (45 gauss/cm max). Radio frequency pulses were applied using a standard transmit/receive volume coil (72-mm internal diameter) actively decoupled from the two-channel Bruker quadrature receiver coil positioned over the centerline of the animal skull. Stereotaxic ear bars were used to minimize movement during the imaging procedure. Mouse temperature was maintained at $37 \pm 0.5^\circ\text{C}$ using a pad heated by a recirculating water bath. After positioning using a triplanar fast low angle shot sequence, MR studies were performed using T1-, T2-, and T2*-weighted MRI scans. The following parameters were used to acquire MRI: (1) Standard T1-weighted multi-slice sequence (repetition time [TR]/echo time [ER] = 500/10 ms; 256×256 matrix; 13–15 slices; 1 mm thick; 32-mm field of view [FOV]; number of excitation [NEX] = 4). (2) T2-fluid attenuation inversion recovery sequence (RARE-IR, TI = 2000; TR = 10,000 ms; TE = 36 ms; RARE factor = 8; FOV = 32 mm; 256×256 matrix; 1-mm slice thickness; 15 slices). (3) T2* mapping sequence (2D gradient echo sequence with multiple echoes; TE = 5, 10, 15, 20, 25, and 30 ms; TR = 3,000 ms; FOV = 32 mm; 1-mm slice thickness [15 slices]; 256×256 matrix; NEX = 2). Acquired images were segmented volumetrically using ImageJ software and hematoma volumes were computed. T2*W images were further processed using Bruker software to yield susceptibility-weighted images (Sehgal et al., 2006), providing an alternative method of segmentation and quality control reference for clot volumes. Both hematoma and ventricular volume were determined by drawing irregular regions of interest (ROIs) on all MRI sections containing the lesions/ventricle and the summed values (area) were multiplied by the thickness of the slice to calculate the volume. The analysis was done using ImageJ software.

Parabiosis

Mice were treated with ketofen (2 mg/kg), and anesthetized using a ketamine (100 mg/kg)-xylazine (10 mg/kg) cocktail. Skin on the opposing sides of each mouse was shaved, cleaned, and swabbed with alcohol and betadine solutions. A longitudinal incision was made along the opposing sides of each mouse. Skin around the incision was freed by blunt dissection, and the ventral edges of the incisions were sutured together with 2-0 silk. Femora were exposed by separating surrounding muscles, taking care not to tear muscle or to damage the nerve. Periosteum was scraped off approximately one half of the length of each bone, and the bones were pulled together by suturing twice around the two bones using 2-0 silk. Muscles around the bones

were joined with three deep sutures placed to support the bony union. The scapulae were exposed by removing covering muscles and scraping the periosteum from the exposed surface. Scapulae were joined by suturing through the bones twice using 4-0 silk and taking care not to splinter the bones. Surrounding muscles were joined by suture. Muscles of the thoracic wall and peritoneal walls of the two animals were joined by shallow suture using 4-0 silk to prevent fluid accumulation in the space between animals. Finally, the dorsal edges of the incisions were sutured together. Blood exchange between the parabiotics was confirmed 15 d post-operatively by injecting Evans blue dye intravenously to one parabiotic partner. Blood samples (100 μl) were collected by retro-orbital bleeding of both the partners 40 min after Evans blue injection. Blood samples were centrifuged, and optical density of serum was determined at 625 nm. The rate of exchange between parabiotics is routinely 1–1.5% per minute such that total blood volume of each animal exchanges 15–20 times/d.

Generation of myeloid-specific AMPK α 1 knockout mice

LysM^{Cre} mice (B6.129P2-Lyz2^{tm1(Cre)lgo}/J; Jackson Laboratories, stock no. 004781), which harbor a nuclear localized Cre recombinase inserted into the first coding ATP of the *Lysozyme 2* gene, were mated with AMPK α 1^{f/f} mice (Prkaa1^{tm1/1Sjm}/J; Jackson Laboratories, stock no. 014141), which possess loxP sites flanking exon 3 of the *AMPK α 1* gene. AMPK α 1^{f/f} mice were backcrossed to C57BL/6J mice for at least 10 generations. Successful mating was confirming by PCR genotyping and by flow cytometry analysis of AMPK expression in myeloid cells. Littermates were used in all experimental procedures

Bone marrow chimeras

C57BL/6J or CD36^{-/-} (B6.129S1-CD36^{tm1Mfe}/J; Jackson Laboratories, stock no. 019006) recipient mice were whole-body irradiated with sub-lethal dose of 6 Gy (Cs137). After 24 h, recipient mice were intravenously injected with 5×10^6 bone marrow cells collected from WT or CD36^{-/-}, as detailed by our laboratory (Braun et al., 2017). Beginning at 2 wk after transplantation, 10 μl of blood was collected from the orbital sinus and CD36 expression was measured in peripheral blood using flow cytometry. Blood from C57BL/6J mice without irradiation or cell transplantation was used as a control. Efficient (>75%) engraftment of bone marrow was present by day 28. On day 30, mice were subjected to sham/ICH.

Preparative and analytic flow cytometry

Freshly harvested brain tissue (0.2 g) was sieved through a 100- μM cell strainer, followed by centrifugation (1,500 rpm, 10 min) to prepare single-cell suspensions. Blood (200 μl) was collected via cardiac puncture or via the retro-orbital sinus. Cells were incubated with antibodies against the following conjugated cell surface markers: CD11b (BD Biosciences, 557396, Clone M1/70), F4/80 (BD Biosciences, 565613, Clone T45-2342), CD206 (BD Biosciences, Cat 565250, Clone MR5D3), MerTK (eBioScience, 12-5751-82, Clone DS5MMER), CD68 (BioLegend, 137010, Clone FA-11), CD36, (BioLegend, 102604, Clone HM36), MHC-II (Novus, NBP1-28161, Clone NIMR-4), Ly-6G (BioLegend, 127603, Clone 1A8), and Ly-6C (BioLegend, 128021, Clone HK1.4). Fol-

lowing a PBS wash, cells were fixed and permeabilized using a Fixation/Permeabilization Concentrate (Affymetrix eBioscience) and then incubated with antibodies for intracellular labeling of phosphorylated AMPK $_{\alpha 1/2}^{\text{Thr183/Thr172}}$ (Bioss, bs-4002R-Cy7), IL-10 (BioLegend, 505009, Clone JES5-16E3), or TNF- α (BD Biosciences, 560659). After a final wash, cells were analyzed using a four-color flow cytometer (FACSCalibur, BD Biosciences), and CellQuest software (BD Biosciences), as we described previously (Braun et al., 2017). Isotype-matched controls were analyzed to set the appropriate gates for each sample. For each marker, samples were analyzed in duplicate. To minimize false-positive events, the number of double-positive events detected with the isotype controls was subtracted from the number of double-positive cells stained with corresponding antibodies (not isotype control), respectively. Viable cells were visibly differentiated from debris by gating on live cells with high forward scatter (FSC) and positivity for specific antibodies. Single stains were performed for compensation controls, controls to check for fluorescence spread, and isotype controls were used to determine the level of nonspecific binding. Cells expressing a specific marker were reported as a percentage of the number of gated events.

Macrophage depletion

A clodronate macrophage depletion kit, containing control liposomes (Encapsome) and clodronate liposomes (Clodrosome; Encapsala NanoSciences), was used to deplete endogenous myeloid cells. Intraperitoneal administration of 200 μ l of placebo or clodronate liposomes (5 mg/ml) was performed once daily for three consecutive days. At 24 h after the final injection, blood was collected via the retro-orbital sinus, and myeloid cell (CD11b $^+$, F4/80 $^+$) depletion was confirmed by flow cytometry, per our laboratory (Braun et al., 2017). Depletion rates >90–95% were routinely achieved using this approach. Sham or ICH was induced upon the confirmation of myeloid cell depletion.

Adoptive transfer of CFSE-labeled macrophages

Total splenocytes and bone marrow were collected, enriched, and CD11b $^+$ CD68 $^+$ F4/80 $^+$ macrophages were consecutively sorted three times by magnetic bead isolation (Miltenyi Biotec) to achieve >95% purity. Purified macrophages were labeled with 5 μ M CFSE (Molecular Probes), a green fluorescent cell staining dye, and resuspended in sterile PBS, as we described (Sharma et al., 2010). A total of 6×10^5 cells/mouse were injected via the tail vein immediately after sham/ICH. Trafficking and phenotypic assessment of adoptively transferred CFSE $^+$ macrophages were analyzed by flow cytometry. Toward this end, 100 μ l of blood or 0.2 mg brain tissue was collected from deeply anesthetized mice via cardiac puncture and assessed by flow cytometry, as detailed above.

Western blotting

Whole cell lysates were prepared from 3-mm coronal sections centered upon the hematoma site and collected in radioimmunoprecipitation assay buffer. Protein concentrations were quantified using a BCA Protein Assay kit (Thermo Scientific), according to manufacturer's guideline. Equal amounts of protein (40 μ g)

were resolved in 10% SDS–polyacrylamide gels and transferred onto a nitrocellulose membrane. Blots were incubated overnight at 4°C in primary antibody 1:1,000 anti-AMPK α (Cell Signaling Technologies, 2532); 1:1,000 anti-phospho-AMPK α^{Thr172} (Cell Signaling Technology, 2535); or 1:8,000 anti- β -actin (Sigma-Aldrich) followed by a 1-h incubation at room temperature with HRP-conjugated anti-rabbit or anti-mouse secondary antibody (Jackson ImmunoResearch). Blots were visualized using ECL Plus Western Blotting Detection System (Biorad), and densitometry analysis was performed using ImageJ software.

Behavioral tests

Neurological scoring

Neurological injury was determined using a modified 24-point scale, as detailed by our laboratory after ICH (King et al., 2011). This scale is comprised of six behavioral tests, each of which is graded from 0 (performs with no impairment) to 4 (severe impairment). A composite score was calculated as the sum of the grades on all six tests. Two investigators blinded to experimental treatment groups scored all data independently.

Elevated body swing test

Animals were held 1 cm from the base of the tail and suspended 1–5 cm above a flat surface. One swing was recorded for each suspension. A swing was defined as a >10 degree deflection from body midline or rotation about the vertical axis. Mice were placed onto the surface between suspensions, allowed to visibly reposition so that no side preferences were observed, and then resuspended. The evaluator varied the hand and standing position, and the testing area was devoid of visual cues to avoid biasing the direction of swings. 20 swings were recorded per trial, and side preference was calculated as swings to one side/total swings.

Narrow beam walk

Motor coordination was evaluated on stationary narrow beam (6 mm wide, 1 m long) over three consecutive days. The first 2 d consisted of training and performance on the beam was quantified on the third day by measuring the time required to traverse the beam. Each mouse was tested three times by a blinded investigator and the average was recorded.

Open field test

Mice were placed in a 40 \times 40 \times 40 cm box for 10 min and activity was digitally recorded. Distance traveled, mean velocity, and time spent in center zone was determined using Ethovision XT video tracking software (Noldus Information Technology).

Hanging wire test

Grip strength was assessed by placing mice on an apparatus consisting of a 50-cm string pulled between two vertical supports. Mice were evaluated as follows: 0, falls off; 1, hangs onto string by two forepaws; 2, same as for 1 but attempts to climb on string; 3, hangs onto string by two forepaws plus one or both hind limbs; 4, hangs onto string by forepaws with tail wrapped around string; and 5, escapes. The highest reading of three successive trials was taken for each animal.

White matter injury

Mice were transcardially perfused with saline, and brains were removed and placed in chilled buffered formalin (10%). Luxol fast blue (LFB) staining was performed to detect white matter fiber density and myelin loss, as detailed by our laboratory (Khan et al., 2015). Tissue sections were imaged using a Keyence BZ-X700 microscope and converted to 16-bit grayscale, and then binary images were created using NIH ImageJ software (0-white, 255-black; threshold value, 129). The mean integrated density of LFB staining was quantified by randomly selecting five ROIs within the white matter tract. The mean integrated density of the background was subtracted from each ROIs. White matter lesions also were visually graded, as previously detailed (Wakita et al., 1995). White matter was assessed by three independent investigators that were blinded to experimental groups. Scoring criteria were normal (Grade 0), disarrangement of nerve fibers (Grade 1), formation of marked vacuoles (Grade 2), or disappearance of myelinated fibers (Grade 3).

Statistical analysis

All data comparisons were made using GraphPad Prism software. Student's *t* tests were used for two-group comparisons. ANOVA followed by Tukey's post-hoc test was used for multiple group comparisons. Data are expressed as mean ± SEM. A *P* value of <0.05 was considered to be significant.

Online supplemental material

Fig. S1 demonstrates the placement and validation of RIC. Fig. S2 shows that RIC does not reduce initial hematoma size after ICH. Fig. S3 demonstrates that RIC-induced hematoma resolution is lost in CCR2^{-/-} mice. Fig. S4 indicates the breeding strategy used to generate myeloid-specific AMPK α 1 knockout mice. Fig. S5 shows AMPK α 1-dependent motor improvements by RIC after collagenase-induced ICH.

Acknowledgments

The authors thank Colby Polonsky for providing illustrations.

Financial support for this project was provided by grants from the National Institutes of Health (grants NS065172, NS095154, NS075774, NS084228, and NS097825) and American Heart Association (GRNT33700286) to K.M. Dhandapani and from the National Institutes of Health (grants NS099455 and NS090609) to D.C. Hess.

The authors declare no competing financial interests.

Author contributions: K. Vaibhav, M. Braun, B. Baban, M.N. Hoda, and K.M. Dhandapani conceptualized, designed, and performed experiments, analyzed data, and wrote the manuscript. M.B. Khan and Z.T. Khan performed RIC and assisted with the performance and analysis of behavioral tasks. R.B.S. Harris, S. Fatima, and M.N. Hoda performed the autologous blood model and the parabiosis experiments. N. Saad and B. Baban performed flow cytometry experiments. A. Shankar and A.S. Arbab acquired and assisted with the analysis of MRI data. Y. Huo and Q. Yan bred myeloid-specific AMPK mice and contributed toward data analysis. S. Giri assessed AMPK subunits in macrophages and contributed toward data analysis. J.R. Vender,

D.C. Hess, and C.H. Alleyne Jr. assisted with experimental design and data interpretation.

Submitted: 18 October 2017

Revised: 7 May 2018

Accepted: 17 August 2018

References

- Andreka, G., M. Vertesaljai, G. Szantho, G. Font, Z. Piroth, G. Fontos, E.D. Juhasz, L. Szekeley, Z. Szelid, M.S. Turner, et al. 2007. Remote ischaemic postconditioning protects the heart during acute myocardial infarction in pigs. *Heart*. 93:749–752. <https://doi.org/10.1136/hrt.2006.114504>
- Barrett, R.J., R. Hussain, W.M. Coplin, S. Berry, P.M. Keyl, D.F. Hanley, R.R. Johnson, and J.R. Carhuapoma. 2005. Frameless stereotactic aspiration and thrombolysis of spontaneous intracerebral hemorrhage. *Neurocrit. Care*. 3:237–245. <https://doi.org/10.1385/NCC:3:3:237>
- Bhasin, R.R., G. Xi, Y. Hua, R.F. Keep, and J.T. Hoff. 2002. Experimental intracerebral hemorrhage: effect of lysed erythrocytes on brain edema and blood-brain barrier permeability. *Acta Neurochir. Suppl. (Wien)*. 81:249–251.
- Biswas, S.K., and A. Mantovani. 2012. Orchestration of metabolism by macrophages. *Cell Metab.* 15:432–437. <https://doi.org/10.1016/j.cmet.2011.11.013>
- Bøtker, H.E., R. Kharbanda, M.R. Schmidt, M. Böttcher, A.K. Kalltoft, C.J. Terkelsen, K. Munk, N.H. Andersen, T.M. Hansen, S. Trautner, et al. 2010. Remote ischaemic conditioning before hospital admission, as a complement to angioplasty, and effect on myocardial salvage in patients with acute myocardial infarction: a randomised trial. *Lancet*. 375:727–734. [https://doi.org/10.1016/S0140-6736\(09\)62001-8](https://doi.org/10.1016/S0140-6736(09)62001-8)
- Braun, M., K. Vaibhav, N. Saad, S. Fatima, D.W. Brann, J.R. Vender, L.P. Wang, M.N. Hoda, B. Baban, and K.M. Dhandapani. 2017. Activation of Myeloid TLR4 Mediates T Lymphocyte Polarization after Traumatic Brain Injury. *J. Immunol.* 198:3615–3626. <https://doi.org/10.4049/jimmunol.1601948>
- Broderick, J., S. Connolly, E. Feldmann, D. Hanley, C. Kase, D. Krieger, M. Mayberg, L. Morgenstern, C.S. Ogilvy, P. Vespa, et al. Quality of Care and Outcomes in Research Interdisciplinary Working Group. 2007. Guidelines for the management of spontaneous intracerebral hemorrhage in adults: 2007 update: a guideline from the American Heart Association/American Stroke Association Stroke Council, High Blood Pressure Research Council, and the Quality of Care and Outcomes in Research Interdisciplinary Working Group. *Stroke*. 38:2001–2023. <https://doi.org/10.1161/STROKEAHA.107.183689>
- Carroll, K.C., B. Violette, and J. Suttles. 2013. AMPK α 1 deficiency amplifies proinflammatory myeloid APC activity and CD40 signaling. *J. Leukoc. Biol.* 94:1113–1121. <https://doi.org/10.1189/jlb.0313157>
- Chang, C.F., J. Wan, Q. Li, S.C. Renfro, N.M. Heller, and J. Wang. 2017. Alternative activation-skewed microglia/macrophages promote hematoma resolution in experimental intracerebral hemorrhage. *Neurobiol. Dis.* 103:54–69. <https://doi.org/10.1016/j.nbd.2017.03.016>
- Chao de la Barca, J.M., O. Bakhta, H. Kalakech, G. Simard, S. Tamareille, V. Catros, J. Callebaut, C. Gadras, L. Tessier, P. Reynier, et al. 2016. Metabolic Signature of Remote Ischemic Preconditioning Involving a Cocktail of Amino Acids and Biogenic Amines. *J. Am. Heart Assoc.* 5:e003891. <https://doi.org/10.1161/JAHA.116.003891>
- Chiu, D.T., J. van den Berg, F.A. Kuypers, I.J. Hung, J.S. Wei, and T.Z. Liu. 1996. Correlation of membrane lipid peroxidation with oxidation of hemoglobin variants: possibly related to the rates of hemin release. *Free Radic. Biol. Med.* 21:89–95. [https://doi.org/10.1016/0891-5849\(96\)00035-4](https://doi.org/10.1016/0891-5849(96)00035-4)
- Christoforidis, G.A., A. Slivka, Y. Mohammad, C. Karakasis, B. Avutu, and M. Yang. 2007. Size matters: hemorrhage volume as an objective measure to define significant intracranial hemorrhage associated with thrombolysis. *Stroke*. 38:1799–1804. <https://doi.org/10.1161/STROKEAHA.106.472282>
- Crisostomo, P.R., G.M. Wairiuko, M. Wang, B.M. Tsai, E.D. Morrell, and D.R. Meldrum. 2006. Preconditioning versus postconditioning: mechanisms and therapeutic potentials. *J. Am. Coll. Surg.* 202:797–812. <https://doi.org/10.1016/j.jamcollsurg.2005.12.002>
- Darrow, V.C., E.C. Alvord Jr., L.A. Mack, and W.A. Hodson. 1988. Histologic evolution of the reactions to hemorrhage in the premature human infant's brain. A combined ultrasound and autopsy study and a comparison with the reaction in adults. *Am. J. Pathol.* 130:44–58.

- de Lima Portella, R., J. Lynn Bickta, and S. Shiva. 2015. Nitrite Confers Preconditioning and Cytoprotection After Ischemia/Reperfusion Injury Through the Modulation of Mitochondrial Function. *Antioxid. Redox Signal.* 23:307–327. <https://doi.org/10.1089/ars.2015.6260>
- Dennis, M.S. 2003. Outcome after brain haemorrhage. *Cerebrovasc. Dis.* 16(Suppl 1):9–13. <https://doi.org/10.1159/000069935>
- Dennis, M.S., J.P. Burn, P.A. Sandercock, J.M. Bamford, D.T. Wade, and C.P. Warlow. 1993. Long-term survival after first-ever stroke: the Oxfordshire Community Stroke Project. *Stroke.* 24:796–800. <https://doi.org/10.1161/01.STR.24.6.796>
- England, T.J., A. Hedstrom, S. O'Sullivan, R. Donnelly, D.A. Barrett, S. Sarmad, N. Sprigg, and P.M. Bath. 2017. RECAST (Remote Ischemic Conditioning After Stroke Trial): A Pilot Randomized Placebo Controlled Phase II Trial in Acute Ischemic Stroke. *Stroke.* 48:1412–1415. <https://doi.org/10.1161/STROKEAHA.116.016429>
- Fang, H., J. Chen, S. Lin, P. Wang, Y. Wang, X. Xiong, and Q. Yang. 2014. CD36-mediated hematoma absorption following intracerebral hemorrhage: negative regulation by TLR4 signaling. *J. Immunol.* 192:5984–5992. <https://doi.org/10.4049/jimmunol.1400054>
- Flores, J.J., D. Klebe, W.B. Rolland, T. Lekic, P.R. Krafft, and J.H. Zhang. 2016. PPAR γ -induced upregulation of CD36 enhances hematoma resolution and attenuates long-term neurological deficits after germinal matrix hemorrhage in neonatal rats. *Neurobiol. Dis.* 87:124–133. <https://doi.org/10.1016/j.nbd.2015.12.015>
- Foerch, C., K. Arai, G. Jin, K.P. Park, S. Pallast, K. van Leyen, and E.H. Lo. 2008. Experimental model of warfarin-associated intracerebral hemorrhage. *Stroke.* 39:3397–3404. <https://doi.org/10.1161/STROKEAHA.108.517482>
- Gebel, J.M. Jr., E.C. Jauch, T.G. Brott, J. Khoury, L. Sauerbeck, S. Salisbury, J. Spilker, T.A. Tomsick, J. Duldner, and J.P. Broderick. 2002. Relative edema volume is a predictor of outcome in patients with hyperacute spontaneous intracerebral hemorrhage. *Stroke.* 33:2636–2641. <https://doi.org/10.1161/01.STR.0000035283.34109.EA>
- Geng, X., C. Ren, T. Wang, P. Fu, Y. Luo, X. Liu, F. Yan, F. Ling, J. Jia, H. Du, et al. 2012. Effect of remote ischemic preconditioning on an intracerebral hemorrhage stroke model in rats. *Neurol. Res.* 34:143–148. <https://doi.org/10.1179/1743132811Y.0000000073>
- Gonzalez, N.R., R. Hamilton, A. Bilgin-Freiert, J. Dusick, P. Vespa, X. Hu, and S. Asgari. 2013. Cerebral hemodynamic and metabolic effects of remote ischemic preconditioning in patients with subarachnoid hemorrhage. *Acta Neurochir. Suppl. (Wien).* 115:193–198.
- Gonzalez, N.R., M. Connolly, J.R. Dusick, H. Bhakta, and P. Vespa. 2014. Phase I clinical trial for the feasibility and safety of remote ischemic conditioning for aneurysmal subarachnoid hemorrhage. *Neurosurgery.* 75:590–598, discussion:598. <https://doi.org/10.1227/NEU.0000000000000514>
- Gordon, S., and F.O. Martinez. 2010. Alternative activation of macrophages: mechanism and functions. *Immunity.* 32:593–604. <https://doi.org/10.1016/j.immuni.2010.05.007>
- Gregson, B.A., J.P. Broderick, L.M. Auer, H. Batjer, X.C. Chen, S. Juvela, L.B. Morgenstern, G.C. Pantazis, O.P. Teernstra, W.Z. Wang, et al. 2012. Individual patient data subgroup meta-analysis of surgery for spontaneous supratentorial intracerebral hemorrhage. *Stroke.* 43:1496–1504. <https://doi.org/10.1161/STROKEAHA.111.640284>
- Hammond, M.D., Y. Ai, and L.H. Sansing. 2012. Gr1+ Macrophages and Dendritic Cells Dominate the Inflammatory Infiltrate 12 Hours After Experimental Intracerebral Hemorrhage. *Transl. Stroke Res.* 3(1, S1):s125–s131. <https://doi.org/10.1007/s12975-012-0174-9>
- Han, N., S.J. Ding, T. Wu, and Y.L. Zhu. 2008. Correlation of free radical level and apoptosis after intracerebral hemorrhage in rats. *Neurosci. Bull.* 24:351–358. <https://doi.org/10.1007/s12264-008-0711-4>
- Hemphill, J.C. III, S.M. Greenberg, C.S. Anderson, K. Becker, B.R. Bendok, M. Cushman, G.L. Fung, J.N. Goldstein, R.L. Macdonald, P.H. Mitchell, et al. Council on Clinical Cardiology. 2015. Guidelines for the Management of Spontaneous Intracerebral Hemorrhage: A Guideline for Healthcare Professionals From the American Heart Association/American Stroke Association. *Stroke.* 46:2032–2060. <https://doi.org/10.1161/STR.0000000000000069>
- Hess, D.C., R.A. Blauenfeldt, G. Andersen, K.D. Hougaard, M.N. Hoda, Y. Ding, and X. Ji. 2015. Remote ischaemic conditioning—a new paradigm of self-protection in the brain. *Nat. Rev. Neurol.* 11:698–710. <https://doi.org/10.1038/nrneuro.2015.223>
- Hess, D.C., M.N. Hoda, and M.B. Khan. 2016. Humoral Mediators of Remote Ischemic Conditioning: Important Role of eNOS/NO/Nitrite. *Acta Neurochir. Suppl. (Wien).* 121:45–48. https://doi.org/10.1007/978-3-319-18497-5_8
- Hoda, M.N., S. Siddiqui, S. Herberg, S. Periyasamy-Thandavan, K. Bhatia, S.S. Hafez, M.H. Johnson, W.D. Hill, A. Ergul, S.C. Fagan, and D.C. Hess. 2012. Remote ischemic preconditioning is effective alone and in combination with intravenous tissue-type plasminogen activator in murine model of embolic stroke. *Stroke.* 43:2794–2799. <https://doi.org/10.1161/STROKEAHA.112.660373>
- Hougaard, K.D., N. Hjort, D. Zeidler, L. Sørensen, A. Nørgaard, T.M. Hansen, P. von Weitzel-Mudersbach, C.Z. Simonsen, D. Damgaard, H. Gottrup, et al. 2014. Remote ischemic preconditioning as an adjunct therapy to thrombolysis in patients with acute ischemic stroke: a randomized trial. *Stroke.* 45:159–167. <https://doi.org/10.1161/STROKEAHA.113.001346>
- Huang, F.P., G. Xi, R.F. Keep, Y. Hua, A. Nemoianu, and J.T. Hoff. 2002. Brain edema after experimental intracerebral hemorrhage: role of hemoglobin degradation products. *J. Neurosurg.* 96:287–293. <https://doi.org/10.3171/jns.2002.96.2.0287>
- Huffman, L.J., P.R. Miles, X. Shi, and L. Bowman. 2000. Hemoglobin potentiates the production of reactive oxygen species by alveolar macrophages. *Exp. Lung Res.* 26:203–217. <https://doi.org/10.1080/019021400269871>
- Joseph, M.J., J. Caliaiperumal, and L.C. Schlichter. 2016. After Intracerebral Hemorrhage, Oligodendrocyte Precursors Proliferate and Differentiate Inside White-Matter Tracts in the Rat Striatum. *Transl. Stroke Res.* 7:192–208. <https://doi.org/10.1007/s12975-015-0445-3>
- Khan, M.B., M.N. Hoda, K. Vaibhav, S. Giri, P. Wang, J.L. Waller, A. Ergul, K.M. Dhandapani, S.C. Fagan, and D.C. Hess. 2015. Remote ischemic postconditioning: harnessing endogenous protection in a murine model of vascular cognitive impairment. *Transl. Stroke Res.* 6:69–77. <https://doi.org/10.1007/s12975-014-0374-6>
- Khan, M.B., S. Hafez, M.N. Hoda, B. Baban, J. Wagner, M.E. Awad, H. Sangabathula, S. Haigh, M. Elsalanty, J.L. Waller, and D.C. Hess. 2018. Chronic Remote Ischemic Conditioning Is Cerebroprotective and Induces Vascular Remodeling in a VCID Model. *Transl. Stroke Res.* 9:51–63. <https://doi.org/10.1007/s12975-017-0555-1>
- Kim, C.K., S.H. Lee, B.J. Kim, W.S. Ryu, S.H. Choi, B.H. Oh, and B.W. Yoon. 2011. Elevated leukocyte count in asymptomatic subjects is associated with a higher risk for cerebral white matter lesions. *Clin. Neurol. Neurosurg.* 113:177–180. <https://doi.org/10.1016/j.clineuro.2010.10.013>
- King, M.D., D.J. McCracken, F.M. Wade, S.E. Meiler, C.H. Alleyne Jr., and K.M. Dhandapani. 2011. Attenuation of hematoma size and neurological injury with curcumin following intracerebral hemorrhage in mice. *J. Neurosurg.* 115:116–123. <https://doi.org/10.3171/2011.2.JNS10784>
- Koch, S., M. Katsnelson, C. Dong, and M. Perez-Pinzon. 2011. Remote ischemic limb preconditioning after subarachnoid hemorrhage: a phase Ib study of safety and feasibility. *Stroke.* 42:1387–1391. <https://doi.org/10.1161/STROKEAHA.110.605840>
- Kröllner-Schön, S., T. Jansen, F. Hauptmann, A. Schüler, T. Heeren, M. Hausding, M. Oelze, B. Viollet, J.F. Keaney Jr., P. Wenzel, et al. 2012. α 1AMP-activated protein kinase mediates vascular protective effects of exercise. *Arterioscler. Thromb. Vasc. Biol.* 32:1632–1641. <https://doi.org/10.1161/ATVBAHA.111.243980>
- Lai, Y.C., D.M. Tabima, J.J. Dube, K.S. Hughan, R.R. Vanderpool, D.A. Goncharov, C.M. St Croix, A. Garcia-Ocaña, E.A. Goncharova, S.P. Tofovic, et al. 2016. SIRT3-AMP-Activated Protein Kinase Activation by Nitrite and Metformin Improves Hyperglycemia and Normalizes Pulmonary Hypertension Associated With Heart Failure With Preserved Ejection Fraction. *Circulation.* 133:717–731.
- Lee, S.H., B.J. Kim, W.S. Ryu, C.K. Kim, N. Kim, B.J. Park, and B.W. Yoon. 2010. White matter lesions and poor outcome after intracerebral hemorrhage: a nationwide cohort study. *Neurology.* 74:1502–1510. <https://doi.org/10.1212/WNL.0b013e3181dd425a>
- Letarte, P.B., K. Lieberman, K. Nagatani, R.A. Haworth, G.B. Odell, and T.A. Duff. 1993. Hemin: levels in experimental subarachnoid hematoma and effects on dissociated vascular smooth-muscle cells. *J. Neurosurg.* 79:252–255. <https://doi.org/10.3171/jns.1993.79.2.0252>
- Lou, M., A. Al-Hazzani, R.P. Goddeau Jr., V. Novak, and M. Selim. 2010. Relationship between white-matter hyperintensities and hematoma volume and growth in patients with intracerebral hemorrhage. *Stroke.* 41:34–40. <https://doi.org/10.1161/STROKEAHA.109.564955>
- Lyden, P.D., A. Shuaib, K.R. Lees, A. Davalos, S.M. Davis, H.C. Diener, J.C. Grotta, T.J. Ashwood, H.G. Hardemark, H.H. Svensson, et al. CHANT Trial Investigators. 2007. Safety and tolerability of NXY-059 for acute intracerebral hemorrhage: the CHANT Trial. *Stroke.* 38:2262–2269. <https://doi.org/10.1161/STROKEAHA.106.472746>
- Mangalam, A.K., R. Rattan, H. Suhail, J. Singh, M.N. Hoda, M. Deshpande, S. Fulzele, A. Denic, V. Shridhar, A. Kumar, et al. 2016. AMP-Activated Pro-

- tein Kinase Suppresses Autoimmune Central Nervous System Disease by Regulating M1-Type Macrophage-Th17 Axis. *J. Immunol.* 197:747–760. <https://doi.org/10.4049/jimmunol.1501549>
- Mantovani, A., A. Sica, and M. Locati. 2005. Macrophage polarization comes of age. *Immunity.* 23:344–346. <https://doi.org/10.1016/j.immuni.2005.10.001>
- Marquardt, G., R. Wolff, R.W. Janzen, and V. Seifert. 2005. Basal ganglia haematomas in non-comatose patients: subacute stereotactic aspiration improves long-term outcome in comparison to purely medical treatment. *Neurosurg. Rev.* 28:64–69.
- Mayor, F., A. Bilgin-Freiert, M. Connolly, M. Katsnelson, J.R. Dusick, P. Vespa, S. Koch, and N.R. Gonzalez. 2013. Effects of remote ischemic preconditioning on the coagulation profile of patients with aneurysmal subarachnoid hemorrhage: a case-control study. *Neurosurgery.* 73:808–815, discussion :815. <https://doi.org/10.1227/NEU.0000000000000098>
- McFadden, J.W., and B.A. Corl. 2009. Activation of AMP-activated protein kinase (AMPK) inhibits fatty acid synthesis in bovine mammary epithelial cells. *Biochem. Biophys. Res. Commun.* 390:388–393. <https://doi.org/10.1016/j.bbrc.2009.09.017>
- Mendelow, A.D., B.A. Gregson, H.M. Fernandes, G.D. Murray, G.M. Teasdale, D.T. Hope, A. Karimi, M.D. Shaw, and D.H. Barer. STICH investigators. 2005. Early surgery versus initial conservative treatment in patients with spontaneous supratentorial intracerebral haematomas in the International Surgical Trial in Intracerebral Haemorrhage (STICH): a randomised trial. *Lancet.* 365:387–397. [https://doi.org/10.1016/S0140-6736\(05\)70233-6](https://doi.org/10.1016/S0140-6736(05)70233-6)
- Meng, R., K. Asmaro, L. Meng, Y. Liu, C. Ma, C. Xi, G. Li, C. Ren, Y. Luo, F. Ling, et al. 2012. Upper limb ischemic preconditioning prevents recurrent stroke in intracranial arterial stenosis. *Neurology.* 79:1853–1861. <https://doi.org/10.1212/WNL.0b013e318271f76a>
- Mikita, J., N. Dubourdiou-Cassagno, M.S. Deloire, A. Vekris, M. Biran, G. Raffard, B. Brochet, M.H. Canron, J.M. Franconi, C. Boiziau, and K.G. Petry. 2011. Altered M1/M2 activation patterns of monocytes in severe relapsing experimental rat model of multiple sclerosis. Amelioration of clinical status by M2 activated monocyte administration. *Mult. Scler.* 17:2–15. <https://doi.org/10.1177/1352458510379243>
- Miron, V.E., A. Boyd, J.W. Zhao, T.J. Yuen, J.M. Ruckh, J.L. Shadrach, P. van Wijngaarden, A.J. Wagers, A. Williams, R.J.M. Franklin, and C. Ffrench-Constant. 2013. M2 microglia and macrophages drive oligodendrocyte differentiation during CNS remyelination. *Nat. Neurosci.* 16:1211–1218. <https://doi.org/10.1038/nn.3469>
- Murry, C.E., R.B. Jennings, and K.A. Reimer. 1986. Preconditioning with ischemia: a delay of lethal cell injury in ischemic myocardium. *Circulation.* 74:1124–1136. <https://doi.org/10.1161/01.CIR.74.5.1124>
- Nakamura, T., R.F. Keep, Y. Hua, J.T. Hoff, and G. Xi. 2005. Oxidative DNA injury after experimental intracerebral hemorrhage. *Brain Res.* 1039:30–36. <https://doi.org/10.1016/j.brainres.2005.01.036>
- Nakamura, T., R.F. Keep, Y. Hua, S. Nagao, J.T. Hoff, and G. Xi. 2006. Iron-induced oxidative brain injury after experimental intracerebral hemorrhage. *Acta Neurochir. Suppl. (Wien).* 96:194–198. https://doi.org/10.1007/3-211-30714-1_42
- Nguyen, J.P., P. Decq, P. Brugieres, C. Yepes, E. Melon, A. Gaston, and Y. Kervel. 1992. A technique for stereotactic aspiration of deep intracerebral hematomas under computed tomographic control using a new device. *Neurosurgery.* 31:330–334, discussion :334–335. <https://doi.org/10.1227/00006123-199208000-00019>
- Nishino, Y., T. Miura, T. Miki, J. Sakamoto, Y. Nakamura, Y. Ikeda, H. Kobayashi, and K. Shimamoto. 2004. Ischemic preconditioning activates AMPK in a PKC-dependent manner and induces GLUT4 up-regulation in the late phase of cardioprotection. *Cardiovasc. Res.* 61:610–619. <https://doi.org/10.1016/j.cardiores.2003.10.022>
- O'Neill, L.A., and D.G. Hardie. 2013. Metabolism of inflammation limited by AMPK and pseudo-starvation. *Nature.* 493:346–355. <https://doi.org/10.1038/nature11862>
- Pearce, E.L., and E.J. Pearce. 2013. Metabolic pathways in immune cell activation and quiescence. *Immunity.* 38:633–643. <https://doi.org/10.1016/j.immuni.2013.04.005>
- Qing, W.G., Y.Q. Dong, T.Q. Ping, L.G. Lai, L.D. Fang, H.W. Min, L. Xia, and P.Y. Heng. 2009. Brain edema after intracerebral hemorrhage in rats: the role of iron overload and aquaporin 4. *J. Neurosurg.* 110:462–468. <https://doi.org/10.3171/2008.4.JNS17512>
- Qureshi, A.I., S. Tuhrim, J.P. Broderick, H.H. Batjer, H. Hondo, and D.F. Hanley. 2001. Spontaneous intracerebral hemorrhage. *N. Engl. J. Med.* 344:1450–1460. <https://doi.org/10.1056/NEJM200105103441907>
- Rincon, F., and S.A. Mayer. 2004. Novel therapies for intracerebral hemorrhage. *Curr. Opin. Crit. Care.* 10:94–100. <https://doi.org/10.1097/00075198-200404000-00003>
- Sadrzadeh, S.M., D.K. Anderson, S.S. Panter, P.E. Hallaway, and J.W. Eaton. 1987. Hemoglobin potentiates central nervous system damage. *J. Clin. Invest.* 79:662–664. <https://doi.org/10.1172/JCI112865>
- Sag, D., D. Carling, R.D. Stout, and J. Suttles. 2008. Adenosine 5'-monophosphate-activated protein kinase promotes macrophage polarization to an anti-inflammatory functional phenotype. *J. Immunol.* 181:8633–8641. <https://doi.org/10.4049/jimmunol.181.12.8633>
- Samovski, D., X. Su, Y. Xu, N.A. Abumrad, and P.D. Stahl. 2012. Insulin and AMPK regulate FA translocase/CD36 plasma membrane recruitment in cardiomyocytes via Rab GAP AS160 and Rab8a Rab GTPase. *J. Lipid Res.* 53:709–717. <https://doi.org/10.1194/jlr.M023424>
- Sehgal, V., Z. Delproposito, D. Haddar, E.M. Haacke, A.E. Sloan, L.J. Zamorano, G. Barger, J. Hu, Y. Xu, K.P. Prabhakaran, et al. 2006. Susceptibility-weighted imaging to visualize blood products and improve tumor contrast in the study of brain masses. *J. Magn. Reson. Imaging.* 24:41–51. <https://doi.org/10.1002/jmri.20598>
- Sharma, M.D., D.Y. Hou, B. Baban, P.A. Koni, Y. He, P.R. Chandler, B.R. Blazar, A.L. Mellor, and D.H. Munn. 2010. Reprogrammed foxp3(+) regulatory T cells provide essential help to support cross-presentation and CD8(+) T cell priming in naive mice. *Immunity.* 33:942–954. <https://doi.org/10.1016/j.immuni.2010.11.022>
- Shen, H.Y., J.E. Coelho, N. Ohtsuka, P.M. Canas, Y.J. Day, Q.Y. Huang, N. Rebola, L. Yu, D. Boison, R.A. Cunha, et al. 2008. A critical role of the adenosine A2A receptor in extrastriatal neurons in modulating psychomotor activity as revealed by opposite phenotypes of striatum and forebrain A2A receptor knock-outs. *J. Neurosci.* 28:2970–2975. <https://doi.org/10.1523/JNEUROSCI.5255-07.2008>
- Sukumari-Ramesh, S., C.H. Alleyne Jr., and K.M. Dhandapani. 2012. Astrocyte-specific expression of survivin after intracerebral hemorrhage in mice: a possible role in reactive gliosis? *J. Neurotrauma.* 29:2798–2804. <https://doi.org/10.1089/neu.2011.2243>
- Teenstra, O.P., S.M. Evers, J. Lodder, P. Leffers, C.L. Franke, and G. Blaauw. Multicenter randomized controlled trial (SICHPA). 2003. Stereotactic treatment of intracerebral hematoma by means of a plasminogen activator: a multicenter randomized controlled trial (SICHPA). *Stroke.* 34:968–974. <https://doi.org/10.1161/01.STR.0000063367.52044.40>
- Thiex, R., V. Rohde, I. Rohde, L. Mayfrank, Z. Zeki, A. Thron, J.M. Gilsbach, and E. Uhl. 2004. Frame-based and frameless stereotactic hematoma puncture and subsequent fibrinolytic therapy for the treatment of spontaneous intracerebral hemorrhage. *J. Neurol.* 251:1443–1450. <https://doi.org/10.1007/s00415-004-0554-5>
- Vaibhav, K., P. Shrivastava, R. Tabassum, A. Khan, H. Javed, M.E. Ahmed, F. Islam, M.M. Saffhi, and F. Islam. 2013. Delayed administration of zingerone mitigates the behavioral and histological alteration via repression of oxidative stress and intrinsic programmed cell death in focal transient ischemic rats. *Pharmacol. Biochem. Behav.* 113:53–62. <https://doi.org/10.1016/j.pbb.2013.10.008>
- Wakita, H., H. Tomimoto, I. Akiguchi, and J. Kimura. 1995. Protective effect of cyclosporin A on white matter changes in the rat brain after chronic cerebral hypoperfusion. *Stroke.* 26:1415–1422. <https://doi.org/10.1161/01.STR.26.8.1415>
- Weimar, C., C. Weber, M. Wagner, O. Busse, R.L. Haberl, K.W. Lauterbach, and H.C. Diener. German Stroke Data Bank Collaborators. 2003. Management patterns and health care use after intracerebral hemorrhage: a cost-of-illness study from a societal perspective in Germany. *Cerebrovasc. Dis.* 15:29–36. <https://doi.org/10.1159/000067119>
- Xi, G., K.R. Wagner, R.F. Keep, Y. Hua, G.M. de Courten-Myers, J.P. Broderick, T.G. Brott, and J.T. Hoff. 1998. Role of blood clot formation on early edema development after experimental intracerebral hemorrhage. *Stroke.* 29:2580–2586. <https://doi.org/10.1161/01.STR.29.12.2580>
- Yellon, D.M., and D.J. Hausenloy. 2005. Realizing the clinical potential of ischemic preconditioning and postconditioning. *Nat. Clin. Pract. Cardiovasc. Med.* 2:568–575. <https://doi.org/10.1038/ncpcardio0346>
- Yip, S., and B.R. Sastry. 2000. Effects of hemoglobin and its breakdown products on synaptic transmission in rat hippocampal CA1 neurons. *Brain Res.* 864:1–12. [https://doi.org/10.1016/S0006-8993\(00\)02067-9](https://doi.org/10.1016/S0006-8993(00)02067-9)
- Zhao, X., G. Sun, J. Zhang, R. Strong, W. Song, N. Gonzales, J.C. Grotta, and J. Aronowski. 2007. Hematoma resolution as a target for intracerebral hemorrhage treatment: role for peroxisome proliferator-activated receptor gamma in microglia/macrophages. *Ann. Neurol.* 61:352–362. <https://doi.org/10.1002/ana.21097>

Zhao, X., G. Sun, S.M. Ting, S. Song, J. Zhang, N.J. Edwards, and J. Aronowski. 2015. Cleaning up after ICH: the role of Nrf2 in modulating microglia function and hematoma clearance. *J. Neurochem.* 133:144–152. <https://doi.org/10.1111/jnc.12974>

Zhu, Y.P., J.R. Brown, D. Sag, L. Zhang, and J. Suttles. 2015. Adenosine 5'-monophosphate-activated protein kinase regulates IL-10-mediated anti-inflammatory signaling pathways in macrophages. *J. Immunol.* 194:584–594. <https://doi.org/10.4049/jimmunol.1401024>